

LIBRARY'S COPY

RECEIVED MAR - 5 1986

021270

021688

LISTWANITES AND THEIR RELATIONSHIP TO GOLD MINERALIZATION
AT ERICKSON MINE, BRITISH COLUMBIA, CANADA

A Thesis
Presented to
The Faculty of
Western Washington University

In Partial Fulfillment
Of the Requirements for the Degree
Master of Science

by Eric Dussell
January, 1986

CORDILLERAN GEOLOGY LIBRARY
GEOLOGICAL SURVEY OF CANADA
100 WEST PENDER ST., 5th FLOOR
VANCOUVER, B.C., CANADA
V6B 1R8

CORDILLERAN GEOLOGY LIBRARY
GEOLOGICAL SURVEY OF CANADA
100 WEST PENDER ST., 5th FLOOR
VANCOUVER, B.C., CANADA
V6B 1R8

LISTWANITES AND THEIR RELATIONSHIP TO GOLD
MINERALIZATION AT ERICKSON MINE, BRITISH
COLUMBIA, CANADA

by

Eric Dussell

Accepted in Partial Completion
of the Requirements for the Degree
Master of Science

Sam P. Keeley
Dean of Graduate School

ADVISORY COMMITTEE

Antoni Wodzycki
Co-Chairman

RS Babcock
Co-Chairman

E H Brown

ABSTRACT

"Listwanites" are silica-carbonate metasomatic rocks derived by the hydrothermal alteration of serpentinized ultramafics. Because listwanites host or are spatially associated world-wide with mercury, gold, nickel, cobalt and tungsten deposits, it is probable that they contribute to the process of ore formation.

Erickson Gold Mine, located in northernmost central British Columbia, Canada, contains gold-quartz veins which cut numerous bodies of listwanite. Gold values are frequently higher in those portions of quartz veins which cut or directly underlie a listwanite body. The main objective of this study is to determine how the listwanites at Erickson might have controlled or affected gold mineralization.

From thermodynamic calculations based upon a mineralogical and fluid-inclusion study of the Erickson lodes, it was determined that gold was transported predominantly as the bisulfide complex, $Au(HS^-)_2$ in a moderately saline ore solution.

It is proposed that the ore solution infiltrated and metasomatized bodies of partially serpentinized peridotite, producing a mineralogically zoned rock called "listwanite". Gold precipitation was triggered by a decrease in the sulfur activity resulting from chemical reactions set up by fluid mixing. This process may account for the common association between listwanites and gold-quartz deposits elsewhere.

ACKNOWLEDGEMENTS

This project was financially supported by Erickson Gold Mining Corporation. I greatly value having had the opportunity to work at Erickson and sincerely appreciate the help and support that I have received. Richard Basnett has been especially helpful in supplying maps, reports and information. Thanks also to Dale Sketchley for sending translations of Russian articles and reference lists on listwanites. Conversations with Richard, Dale, Matt Ball, Richard Somerville and Dr. Andre Panteleyev have been very useful as my frequent references to some of them in the text indicates.

I also wish to thank faculty members Dr. Jontek Wodzicki, Dr. Edwin Brown and Dr. Scott Babcock for serving on my thesis committee. Their advice and criticisms are appreciated.

I owe a special debt of gratitude to Rick Somerville, Chief Geologist of Erickson G.M.C. Rick's advice, support and friendship have meant much to me during the six years of our association.

Finally, thanks to my wife Susan who paid the bills and made this paper possible.

TABLE OF CONTENTS

Abstract	i
Acknowledgements	ii
INTRODUCTION	1
Objectives	2
MINE LOCATION AND DESCRIPTION	4
Mine History	4
Previous Research Papers On Erickson	6
TECTONIC SETTING	7
REGIONAL GEOLOGY - MCDAME MAP-AREA	7
MINE GEOLOGY	15
Lithology	15
Structure	16
MINERALOGY AND PETROLOGY	17
GEOCHEMISTRY OF LISTWANITES AT ERICKSON	30
Methods	31
Results	31
Major and Minor Elements	31
Trace Elements	38
FLUID INCLUSION STUDIES	40
Methods	40
Observing Phase Transitions	41
Solid-liquid Phase Transition	42
Vapor-liquid Phase Transition	43
Results	43
Chemical Composition	44
Fluid Temperature, Pressure and Density	47
DISCUSSION	52
Determining the Ore Solution Chemistry	55
Determining the Listwanite Parent Rock Composition	61
Determining the Gold Transport Complex	65
Determining the Serpentinite Fluid Phase Composition	69
Determining the Gold Precipitation Mechanism	73
CONCLUSION	79
REFERENCES CITED	80
APPENDICES	85

LIST OF FIGURES

Figure Number		Page Number
1	Location map of Erickson Gold Mine	5
2	Sketch map of the North American Cordillera	8
3	Generalized map of Cordillera Suspect Terranes	9
4	McDame Map-Area location	11
5	Location and geologic setting of the Sylvester Allocthon	13
6	Sulfide paragenesis of the quartz lodes	20
7	Photograph of Erickson gold ore - Bear Vein	22
8	Photomicrograph illustrating sulfide paragenesis	23
9	Photomicrograph showing gold replacing pyrite and chalcopyrite	24
10	Photomicrograph illustrating gold replacing pyrite and tetrahedrite	25
11	SEM Microphotograph of gold in pyrite	26
12	Photograph of listwanite serpentine-carbonate zone	27
13	Microphotograph of listwanite serpentine-carbonate zone	27
14	Photograph of listwanite talc-carbonate zone	28
15	Microphotograph of listwanite talc-carbonate zone	28
16	Photograph of listwanite quartz-carbonate zone	29
17	Microphotograph of listwanite quartz-carbonate zone	29
18	Listwanite sample locations on 1285 level	32
19	Diagram showing weight percent gains and losses of selected major elements during metasomatism	35
20	Diagram showing weight percent gains and losses of selected major elements for various volume ratios	37
21	Freezing point depression determinations for Alison and Maura Veins	45

22	Diagram showing fusion temperature depression of ice by NaCl	46
23	P-T diagram showing isochore and boiling curve	48
24	Measurements of the temperature of the V-L transition	49
25	Vapor pressure curve for a 10 weight percent NaCl solution	51
26	log f_{O_2} vs pH diagram	56
27	log f_{O_2} vs T diagram	59
28	Regions of stability of some compounds in the system MgO - SiO ₂ - CO ₂ - H ₂ O under standard and hydrothermal conditions	63
29	Change in dissociation constant of water with increasing temperature	67
30	Idealized model of listwanite showing activity gradients during metasomatism	76
31	Diagram illustrating the relative effect of chemical components on gold solubility	78

LIST OF TABLES

Table Number		Page Number
I	Selected equilibrium constants	53
II	Summary of pH determinations for both naturally occurring and synthesized fluids	72
III	Summary of fluid composition calculations	74

LIST OF APPENDICES

Appendix Number		Page Number
I	Chemical analyses for major and minor elements	85
I	Chemical analyses for trace elements	86
II	Fluid-inclusion data	87
III	Petrography of Erickson rocks	89

INTRODUCTION

"Listwanite" (alt. listvenite) is a term coined by A. Holmes in 1928 (Diakow and Panteleyev, 1981) for a predominantly silica-carbonate metasomatic rock containing the chromiferous mica, mariposite. Listwanites characteristically display mineralogical zoning (Shcherban' and Borovikova, 1969) and frequently host a variety of ore minerals (Stul'chikov and others, 1982). Although a comprehensive literature has been amassed in the more than century long period of their study (Shcherban', 1966), the term is not widely used outside the Soviet Union. Analogous terms for listwanites encountered elsewhere in the literature include "quartz-magnesite rock" (Shcherban', 1966, p. 488), "silica-carbonate rock" (Hobbs and Pecora, 1941, p.57), "mariposite rock" (Wittkopp, 1980, p. 13) and "dolomitic vein" (Storms, 1899, p.363).

With few exceptions, Listwanites are formed through the metasomatic alteration of serpentinites. They are "evolved as products of two successive stages of the same process: the serpentinitization of ultrabasites and metasomatic alteration of serpentinites" (Kashkai and Allakhverdiev, 1971, p.6). Listwanites occur as lenses, veins, pods and vein-like bodies within ultramafic formations of the "Alpine-type".

Listwanite research is of practical as well as theoretical importance because listwanites host or are spatially associated world-wide with gold, mercury, nickel, cobalt and tungsten deposits. Due to the distinctively green color imparted to these rocks by chromiferous mica and their general resistance to erosion as a result of silicification, listwanites commonly stand out topographically as highly visible ridges or knobs. This allows geologists to utilize them as an additional prospecting parameter in the search for these deposits (Azimov, 1976).

assemblages.

5. To determine the gold precipitating mechanism. Thermodynamic calculations on data from objective 2 should indicate the cause of gold deposition.

This study involves construction of a chemical and physical model of listwanite metasomatism showing the activity gradients which should exist across a listwanite body during fluid mixing. Although restricted in scope to the Erickson deposit, the mechanism triggering gold precipitation at Erickson may account for the common gold-listwanite association elsewhere.

MINE LOCATION AND DESCRIPTION

Erickson Mine is located 115 kilometers south of Watson Lake, Y.T. in northernmost central British Columbia, Canada (Fig. 1). The town of Cassiar, Brinco's major asbestos mine can be reached by gravel road about 15 kilometers to the west. Erickson ore is mined from 1 - 10 meter thick quartz veins by a modified open stope method. Both gold and silver are recovered from ore shoots in an approximate 1:1 ratio. Gold occurs in the free state and admixed in various sulfides, principally pyrite and tetrahedrite. Silver is present mainly in argentiferous tetrahedrite. To date, a majority of the production has come from five quartz veins, the Jennie, Maura, Bear, Alison and Vollaug.

MINING HISTORY

As is the case with most gold mining districts, placer gold attracted the first prospectors to the area. In 1873, Henry Thiebert made the initial discovery of placer gold in the area in a tributary of Dease Lake. The following year, a prospector named Henry McDame discovered gold in what is today known as "McDame Creek" which drains out of McDame Lake, the present site of the Erickson camp. By 1895, over 70,000 ounces of "reported" gold was recovered from creeks and streams throughout the district (Diakow and Panteleyev, 1981). However, lode gold possibilities were not exploited until 1934 when J.F. Callison staked the first mineral claim on Quartz Creek. A staking rush ensued with the result that, by 1939, most known gold showings had been discovered. About this time, a crosscut was driven into the Jennie Vein but no significant values were intersected. From 1974 through 1978, the Jennie Vein was explored, initially by Agnes and Jennie Mining Co. Ltd., and later as a joint venture

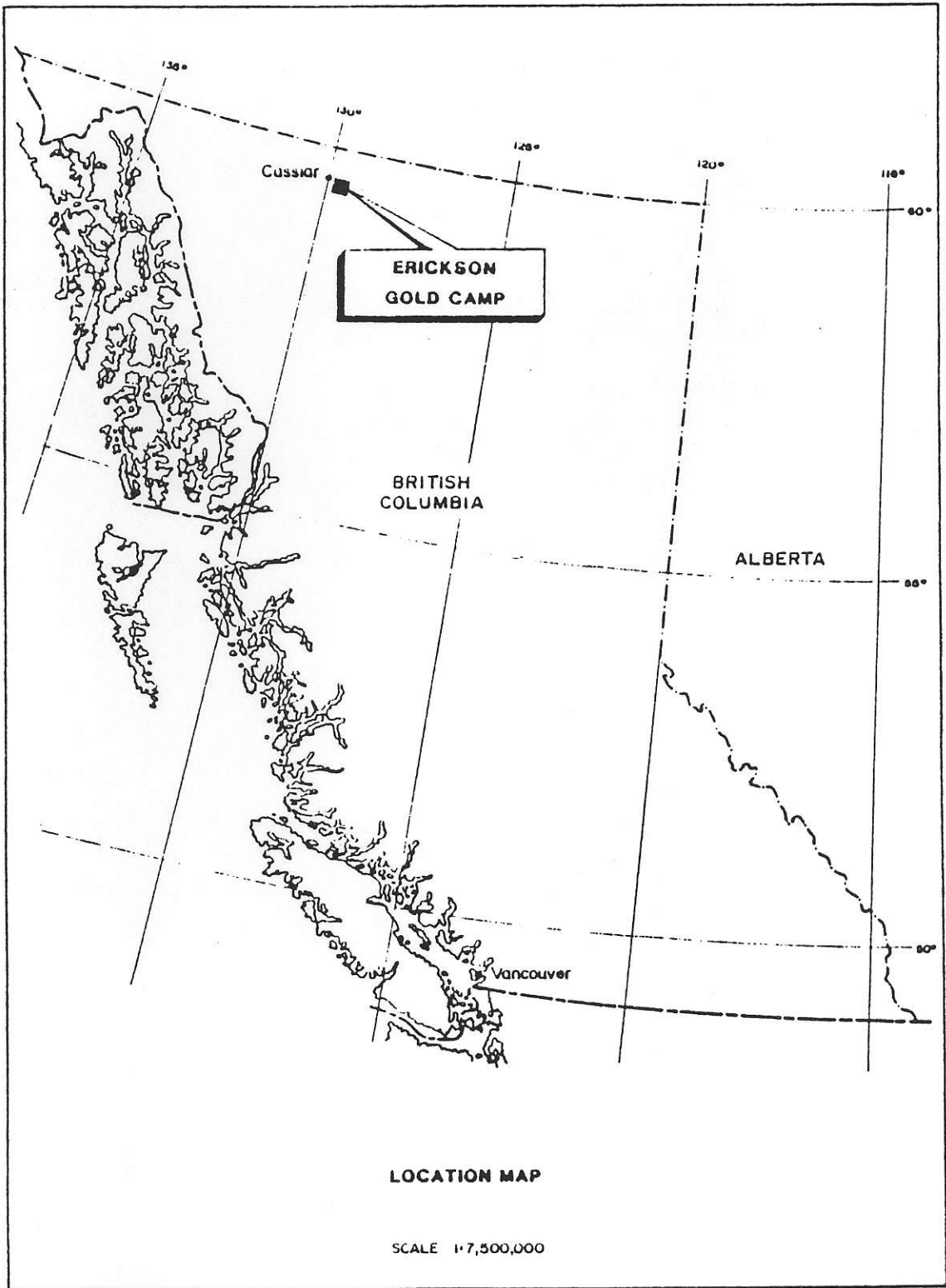


Fig. 1. Location map of Erickson Gold Camp, Cassiar District, B.C.

with Nu Energy Development Corporation. Financing was received and on December 22, 1978, the first ore went to the mill. Initial capacity was 100 tons per day which has since been increased to 300 tons per day. To date, over 320,213 tons have been milled at an average grade of .484 ounces of gold per ton and .420 ounces of silver.

Previous Work on Erickson Mine

The following unpublished research papers have been written on the Erickson deposit:

1. A Microscopy Investigation of the Gold and Sulfides from the Erickson Mine, Cassiar, BC - Gregory Fjetland, December 1982, Senior Thesis, University of British Columbia.
2. Sulfide Mineralogy of the Gold-Quartz Veins at Erickson Gold Camp, Cassiar, BC - D.G. Hooper, 1983, Senior Thesis, University of British Columbia.
3. Preliminary Report on the Mineralogy and Textures of Graphitic Ribbons Characteristic of the Vollaug Vein, Cassiar, BC - D. Sketchley, 1984.
4. Preliminary Report on Wallrock Alteration of Erickson Gold Mine, Cassiar District, by D.A. Sketchley and A.J. Sinclair, Department of Geological Sciences, University of British Columbia, Vancouver, B.C., and R. Somerville, Erickson Gold Mines Ltd., Vancouver, B.C.
5. Preliminary Report on the Alison and Maura Vein Systems, Erickson Gold Mines, Cassiar, B.C., by Paul G. Anderson, Department of Geology, Queens University, Kingston, Ontario, 1985.

TECTONIC SETTING

The Canadian Cordillera is comprised of five physiographically and geologically distinct belts of rock which achieved their present configuration late in the Mesozoic (Monger and others, 1972). They are, from east to west: 1. Rocky Mountain Belt, 2. Omineca Crystalline Belt, 3. Intermontane Belt, 4. Coast Plutonic Complex, and 5. Insular Belt (Figure 2).

Previous discussions on the evolution of the North American Cordillera in the context of geosynclinal theory have been superseded by a plate tectonic model which better accounts for the lithologies, structure and paleomagnetic orientation of these rocks. The North American Cordillera is now recognized as a mosaic of over fifty, fault-bound geologic "terrane" (Figure 3). Over 70 percent of these terranes are "suspect" because their paleogeographic setting with respect to the North American craton cannot be established (Coney and others, 1980). Paleomagnetic studies indicate that northward transport and/or clockwise rotation of these terranes "have been the prime elements in shaping the Cordillera" (Beck, 1980, p.7115).

Erickson Gold Camp is situated within the "E" (Eastern Assemblage) terrane "which includes possible late Precambrian-early Paleozoic metamorphic terranes of possible continental affinity together with Mississippian to Triassic basalt ultramafics and chert and volcanoclastics and carbonates, overlain unconformably by Middle Triassic to Lower Jurassic volcanogenic strata" (Coney and others, 1980, p.330).

REGIONAL GEOLOGY

Erickson Gold Camp is located within the McDame map-area which covers

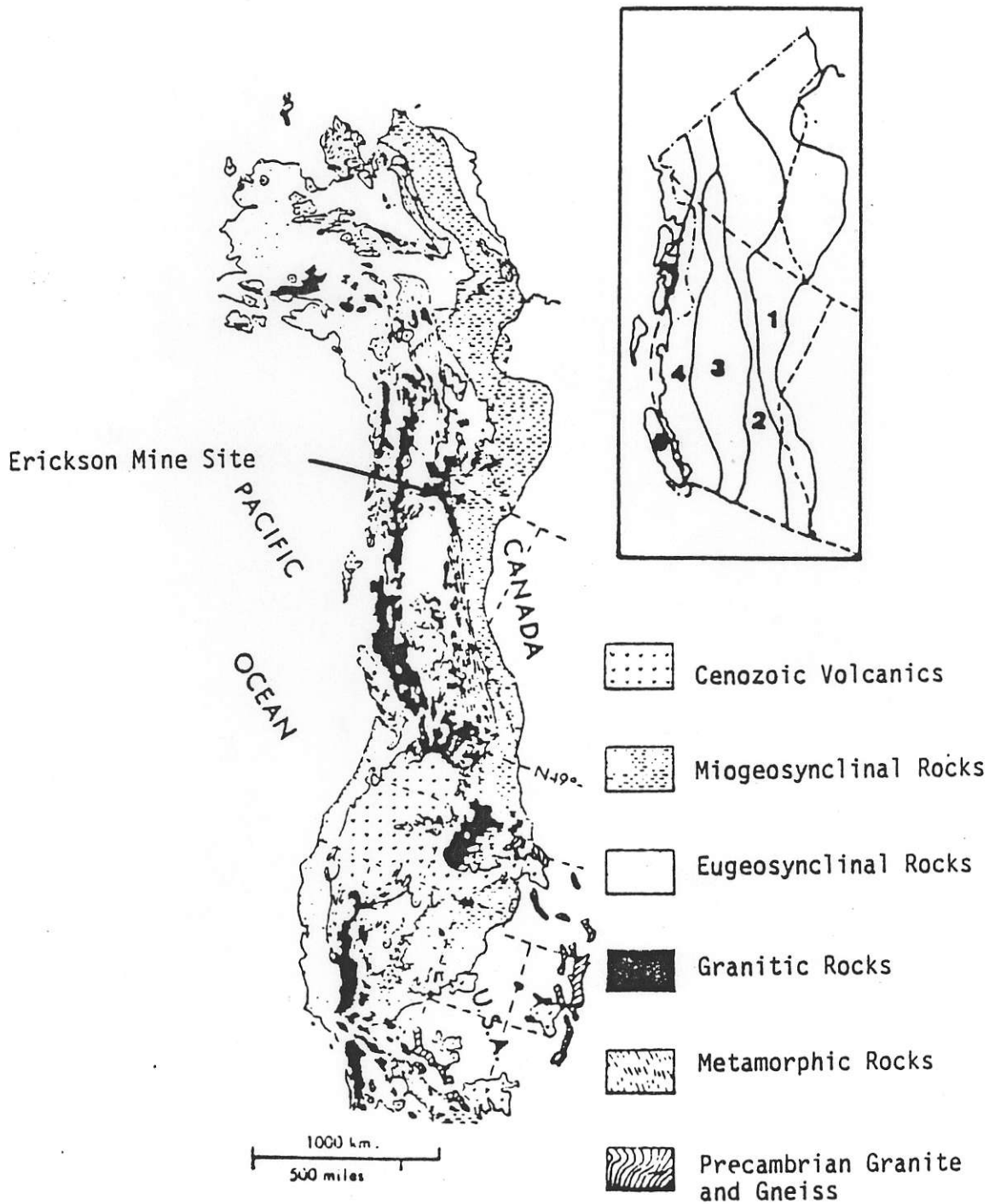


Fig. 2. Sketch map of the North American Cordillera. The inset map shows the location of the geological and physiographic belts of the Canadian Cordillera. These are: (1) Rocky Mountain Belt, (2) Omineca Crystalline Belt, (3) Intermontane Belt, (4) Coast Plutonic Complex, (5) Insular Belt. (After Monger and others, 1972)

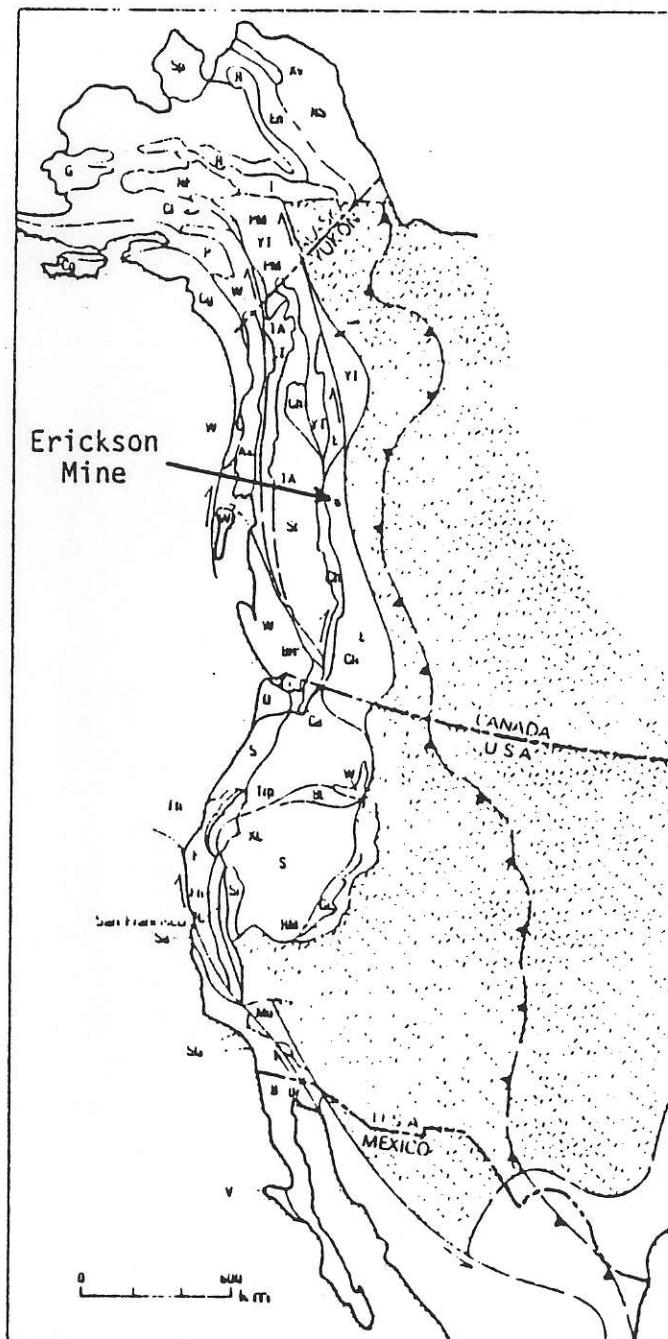


Fig. 3. Generalized map of Cordilleran Suspect Terranes. Dashed pattern, North American autochthonous cratonic basement. (After Coney and others, 1980)

approximately 4,900 square miles in northernmost central British Columbia. It is bounded by the latitudes 59 degrees and 60 degrees and the longitudes 128 degrees and 130 degrees (Figure 4). Initial geological mapping in the area was begun in the summer of 1949 by L.L. Price and continued during the summers of 1950 through 1954 by H. Gabrielse of the Geological Survey of Canada. Gabrielse (1963) summarizes this work in what constitutes the most complete description of the geology to date. Later work has been done by Panteleyev (1979, 1980), Diakow and Panteleyev (1981), and Gordy and others (1982). Somerville and Basnett (1983) describes the geology within the boundaries of the Erickson Gold Camp proper.

The rocks of the McDame map-area are of marine origin and range in age from Proterozoic to Mississippian. Mesozoic granitic rocks intrude the assemblage and Tertiary sediments and basalts occur locally.

The oldest rocks within the McDame map-area are Precambrian and/or Cambrian metasediments of the Horseranch Group which exceed 7,500 feet in thickness. Bounded by faults and glacial drift, their relation to other rocks have not been established.

Good Hope and At^aIn Groups consists of Upper Precambrian to Lower Cambrian limestones, dolomites and sediments exceeding 7,000 feet in thickness.

Conformably overlying these rocks are Middle Cambrian to Middle Ordovician limestones and shales of the Kechika Group which are disconformably overlain by the Sandpile Group.

The Upper Ordovician to Middle Silurian dolomites and cherts of the Sandpile Group are disconformably overlain by Middle and Upper Devonian carbonate rocks of the McDame Group.

The Sylvester Group, a 15,000 ft. thick assemblage of Upper Devonian

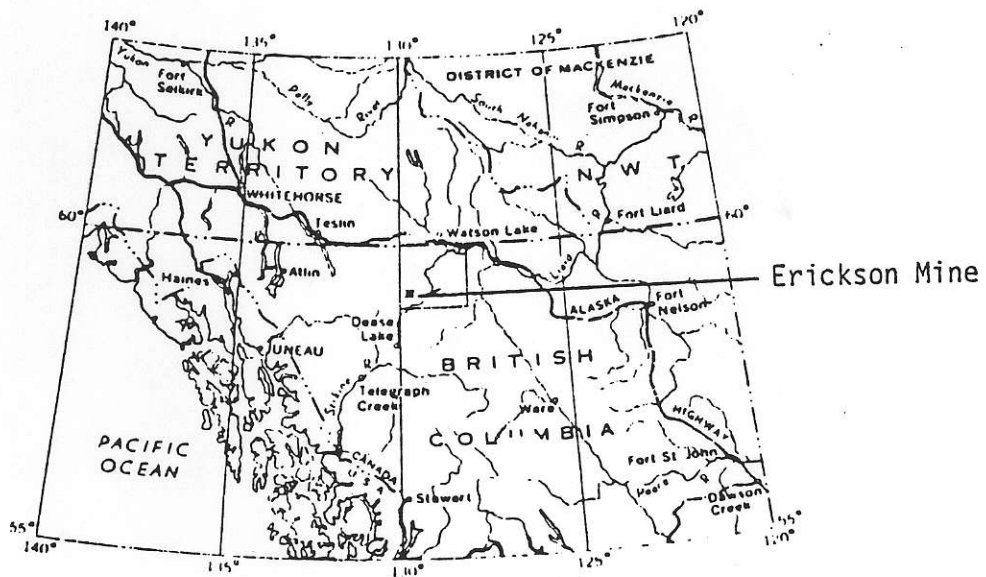


Fig. 4. McDame Map-Area (After Gabrielse, 1963)

and Lower Mississippian volcanics and sediments lies conformably on the McDame Group. These rocks are important because they host the gold-quartz veins of the Erickson Gold Camp. Sylvester Group rocks are characterized by the abundance of volcanic material, chert and impure quartzitic rocks. Massive, medium-grained greenstones are common and are particularly prominent in the vicinity of McDame Lake, the Erickson mine site. Compositionally, the Sylvester greenstones were originally pyroxene andesites and/or basalts (Gabrielse, 1963). Occurring within the Sylvester Group are ultramafic rocks of probable Mississippian age. The compositions of the ultramafics include dunite, pyroxenite and peridotite. These rocks occur as a linear belt, the "McDame ultramafic belt" (Gabrielse, 1963, p.63.) and are restricted in occurrence to the Sylvester Allocthon.

The Sylvester Allocthon, (Figure 5), in southwestern McDame map-area, is composed of at least three, discrete, fault-bound assemblages of Sylvester Group sediments and volcanics which were overthrust and lie above autochthonous strata of the North American miogeocline (Gordy and others, 1982). The Erickson lodes are restricted in occurrence to the greenstones of the basal thrust sheet which also contains chert, shale, serpentinite and intrusive (diorite and/or gabbro).

Unconformably overlying Sylvester Group rocks are the well-bedded, predominantly carbonate succession of the Nizi Formation which are of Mississippian age.

Granitic rocks of the Cassiar and Four Mile batholiths were probably emplaced in the Jura-Cretaceous time (Gabrielse, 1963).

A few small outcrops of Tertiary or possibly Pleistocene extrusive rocks occur along the Blue River. A thick blanket of quaternary glacial

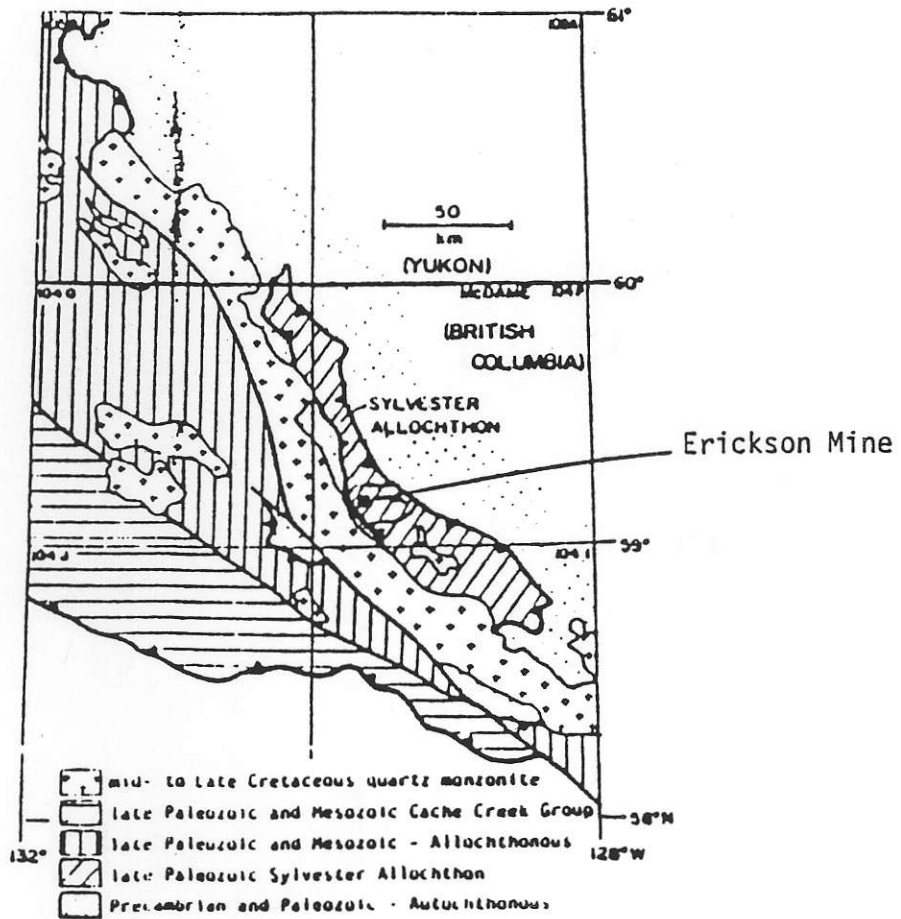


Fig. 5. Location and geological setting of the Sylvester Allochthon (After Gordy and others, 1982)

drift covers much of the McDame map-area.

MINE GEOLOGY

I. Lithologies:

The orebodies at Erickson Mine are hosted within a package of rocks with oceanic affinity corresponding to Gordy and others (1982) basal thrust sheet of the Sylvester Allocthon. Other lithologies included within this lower thrust sheet are serpentinite, basalt flows and/or pyroclastics, bedded chert, siliceous shale, and small bodies of intrusive gabbro or diorite. Within the general mine area, volcanics greatly predominate in total volume. The gold-quartz veins occur within the volcanics or "greenstones" where they occupy steeply-dipping, cymoidal - shaped fractures and/or faults which commonly splay downward off the listwanite-greenstone contact. "Greenstone" is a collective term used by Gabrielse (1963, p.61) for the characteristically massive, medium-grained and medium to dark green Sylvester Group volcanics in the vicinity of McDame lake, the Erickson mine-site. Both flow-type extrusive and pyroclastic rocks are represented. The green color of the volcanics is imparted by the metamorphic mineral assemblage, chlorite-actinolite-epidote. The average composition of these rocks is believed to be andesitic by the Erickson geologists, although this is difficult to determine because of metamorphic recrystallization and extensive hydrothermal alteration.

The quartz veins average a few meters in thickness but can attain dimensions approaching 10 meters. Vein structures and mineralogy approximate Lindgren's "mesothermal" category (Park and MacDiarmid, 1975, p. 311). The gold-ore is mined from shoots with a commonly predictable rake within the plane of the vein.

Black graphitic argillite appears to have been thrust faulted on top

of the volcanic pile and is seldom encountered within the mine workings. This unit may be the basal member of Gordy and others (1982) upper thrust sheet which he terms a black shale.

The quartz veins at Erickson frequently crosscut a zoned, quartz-carbonate metasomatic rock referred to as "listwanite" by S.F. Leaming after a term coined by A. Holmes in 1928 (Diakow and Panteleyev, 1981). These bodies average 30 meters in thickness, appear largely concordant, and are composed of mineral assemblages typical of metamorphosed ultrabasic rocks, viz., talc, serpentine, magnesite and chromiferous mica.

Numerous Tertiary diabase dikes cut the rocks throughout the mine area.

II. Structure:

Rocks within which the Erickson camp is situated have been subjected to at least two and possibly three folding events and are transected by both thrust and steep normal transverse faults with considerable offset (Diakow and Panteleyev, 1981). The gold-quartz veins at Erickson mine dip steeply and trend consistently to the northeast. Somerville and Basnett (1983, p.43) interpret the vein structures as "located within a shallow, open, northwesterly-trending synclinal basin which has been cross-folded along two westerly striking anticlinal axes. The north-dipping Jennie, Alison and Maura veins are situated on the southern limb; the Dease, Bear, and Goldie veins dip south on the northern limb of this basin structure".

MINERALOGY AND PETROLOGY

I. Volcanics:

Gabrielse (1963) characterizes Sylvester Group volcanics as massive, fine to medium-grained greenstones which can be subdivided microscopically into three types which grade into one another in the field. A pyroxene andesite or basalt parent rock is indicated for all types on the basis of the mineralogy, textures and geochemistry of these rocks (Gabrielse, 1963). Original ophitic and subophitic textures of uralitized diopsidic-augite and labradorite are altered to various mineral assemblages including the minerals, tremolite, actinolite, zoisite, clinozoisite, albite, calcite, chlorite, leucoxene, sphene and ilmenite.

Within the area of the Erickson mine-site, Somerville and Basnett (1983) subdivide the volcanics into the following units:

A. Andesite to Dacite Flows: In hand specimen, these rocks are characteristically massive, fine grained and medium to dark green in color. Pillow structures represent the dominant criteria for distinguishing this rock unit. Extensive alteration has largely obliterated the original textures and mineralogy of the volcanics although a few relict grains of plagioclase and pyroxene have survived. The corroded phenocrysts of clinopyroxene and lesser orthopyroxene typically show alteration to chlorite and fine-grained bundles of actinolitic amphibole. Relict laths of plagioclase are commonly poikilitic, containing inclusions of chlorite and epidote. The groundmass is characteristically altered to the assemblage, chlorite-epidote-actinolite-calcite-opaque oxide which corresponds to greenschist facies metamorphism (Turner, 1981). Extensive hydrothermal alteration is evidenced by

replacement patches and veinlets of quartz, dolomite and sericite.

B. Andesite to Dacite Tuff Breccia: Thin, reticulate veinlets of chlorite, when highly concentrated, produce a brecciated appearance in the greenstones which is the distinguishing characteristic of this rock category.

C. Argillaceous Tuff: This rock unit is recognizable by its fragmental appearance and the black, graphitic or argillaceous material between the angular volcanic fragments. Carbonate alteration is commonly extensive producing a bleached appearance in hand specimen.

II. Sedimentary Rocks: Included in this category are black, graphitic argillite and pale green chert. The argillite is weakly foliated, commonly pyritic and extensively carbonate altered. Light green chert is easily mistaken for intensely silicified volcanics except where it contains ribbon structure.

III. Diabase Dikes:

Coarse-grained augite and hypersthene occur with zoned plagioclase in a typical diabasic texture. In hand specimen, these rocks appear brownish black, medium to fine grained and commonly show extensive clay alteration.

IV. Quartz Veins:

Quartz veins at Erickson are commonly localized within dilatent zones opened up by faulting and shearing. Continued movement during crystallization of the veins opened conduits for later injections of quartz. A minimum of three quartz generations are clearly recognizable in the lodes and a fourth generation is present in places. The greatest volume of quartz was deposited during the initial generation and appears

milky and relatively barren of sulfides, containing only minor pyrite and sphalerite. The second generation hosts the greatest amount of mineralization including pyrite, tetrahedrite, sphalerite, chalcopyrite and free gold. Galena and arsenopyrite are rare. Second generation quartz is relatively clear. Third generation quartz is clear, smaller in volume, and less well mineralized than second generation quartz. The fourth quartz generation, where it occurs, is smaller in volume than all preceding generations and appears barren of sulfides and gold.

In polished sections of the quartz lodes, gold can be found replacing all of the sulfides although a majority of gold occurs within pyrite. The paragenetic order of the sulfides in all of the veins studied approximates that shown by Figure 6.

V. Listwanite:

The listwanites at Erickson can be characterized as carbonate altered metasomatic rocks containing three distinct mineralogical zones with sharp boundaries. Where the listwanite bodies crosscut quartz veins, the distribution of the mineralogical zones outward from the vein are as follows:

A. Quartz-Carbonate Zone: Rocks of this zone are typically composed of an interlocking mosaic of coarse-grained magnesite and dolomite with lesser replacement patches and interconnecting veinlets of fine to medium-grained quartz. Trace amounts of chromiferous mica impart a distinctive greenish color to the rock similar to a dull copper oxide stain. Antigorite, talc and chlorite also occur in trace amounts. Widely scattered anhedral to subhedral pyrite averages about 1 to 2 percent but can reach concentrations near 5 percent. Of particular importance is the rare occurrence of free gold visible to the naked eye in stringers, veins and

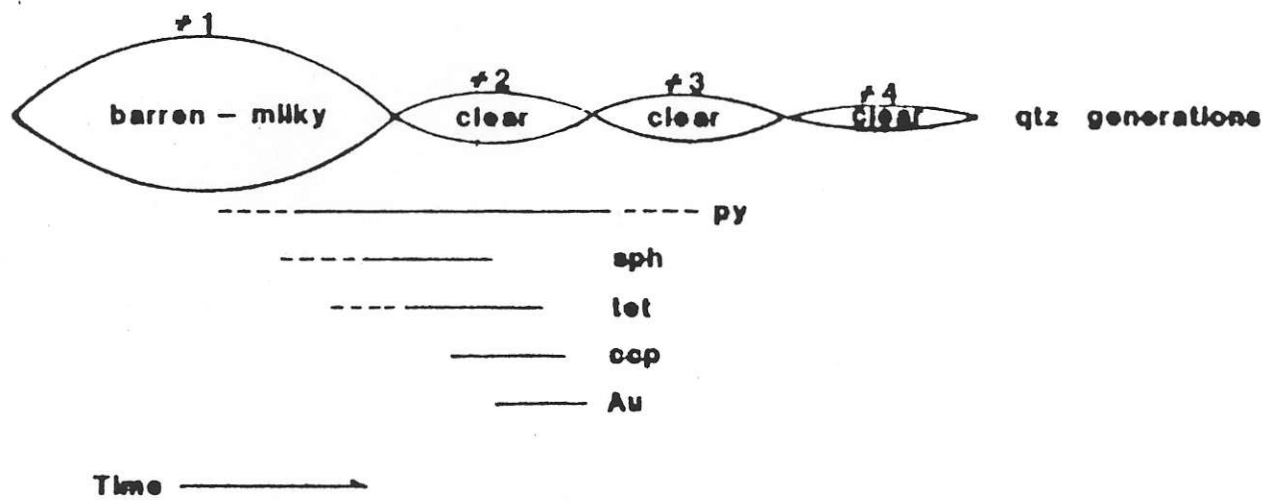


Fig. 6. Sulfide paragenesis of Erickson quartz lodes.

irregular zones of quartz.

B. Talc-Carbonate Zone: In hand specimen, these rocks appear light to medium grey in color and are extremely soft, reflecting the high content of talc. Coarse-grained magnesite and dolomite constitute the other main mineral phase. Small patches of chlorite occur with minor antigorite where replacement has been incomplete. Scattered throughout are small (,0.5 mm) grains of anhedral to subhedral pyrite with a few other minor opaque grains.

C. Serpentine-Carbonate Zone: This mineralogically complex zone is composed predominantly of magnesite, dolomite and antigorite serpentine with subordinate amounts of talc, chlorite and quartz. The opaque minerals ilmenite, chromite, cobaltite, ferrosphenel and other chromium and cobalt minerals are indicated by X-ray diffraction analysis.

Photographs and microphotographs of rocks characteristic of these mineralogical zones are shown in figures 12 through 17 (pp. 27-29).

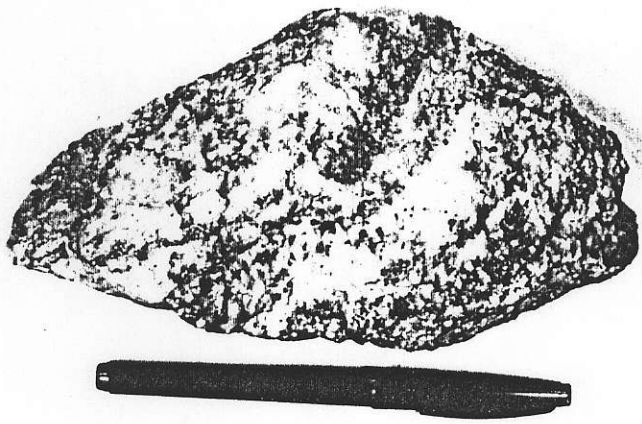


Fig. 7. Erickson gold ore. Sample selected from ore shoot in Bear Vein, 21 level. Fleck of visible gold in lower right.

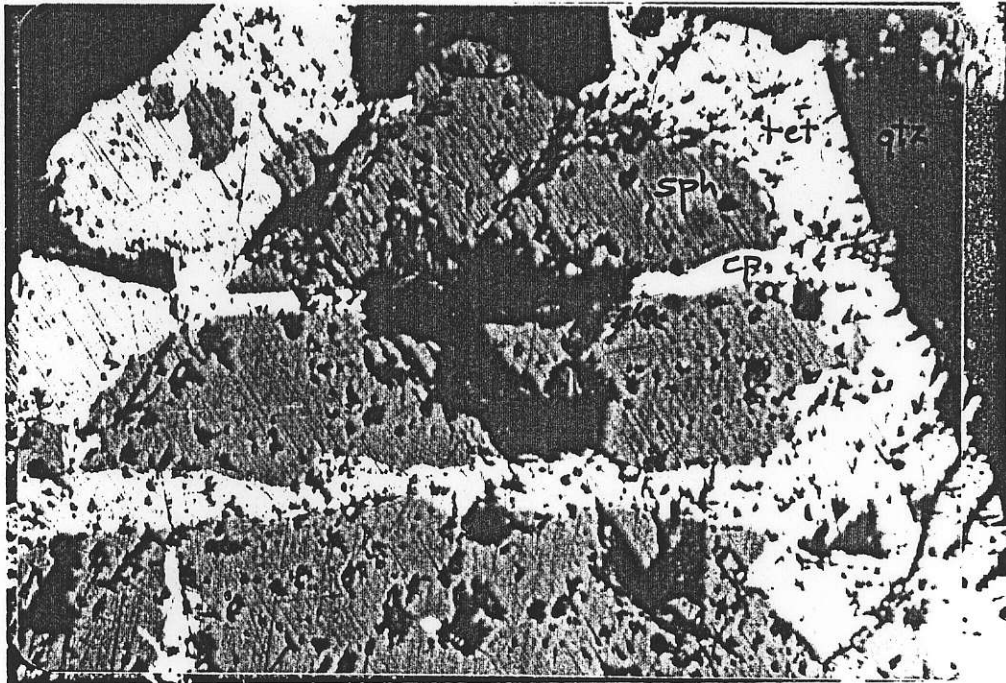


Fig. 8. Sphalerite (sph) rimmed and replaced by tetrahedrite (tet) cut by chalcopyrite (ccp). Bear Vn. Paragenesis is, sph -- tet -- ccp. Mag: 500X

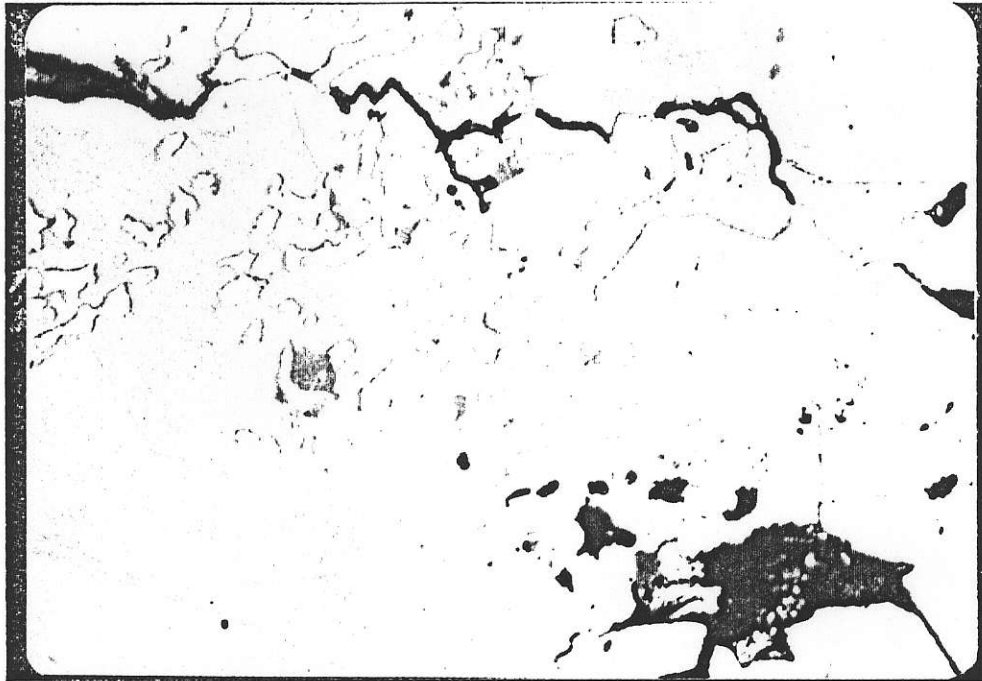


Fig. 9. Gold replacing pyrite and chalcopyrite
(darker grain left of center). Bear Vein.
Mag: 500X

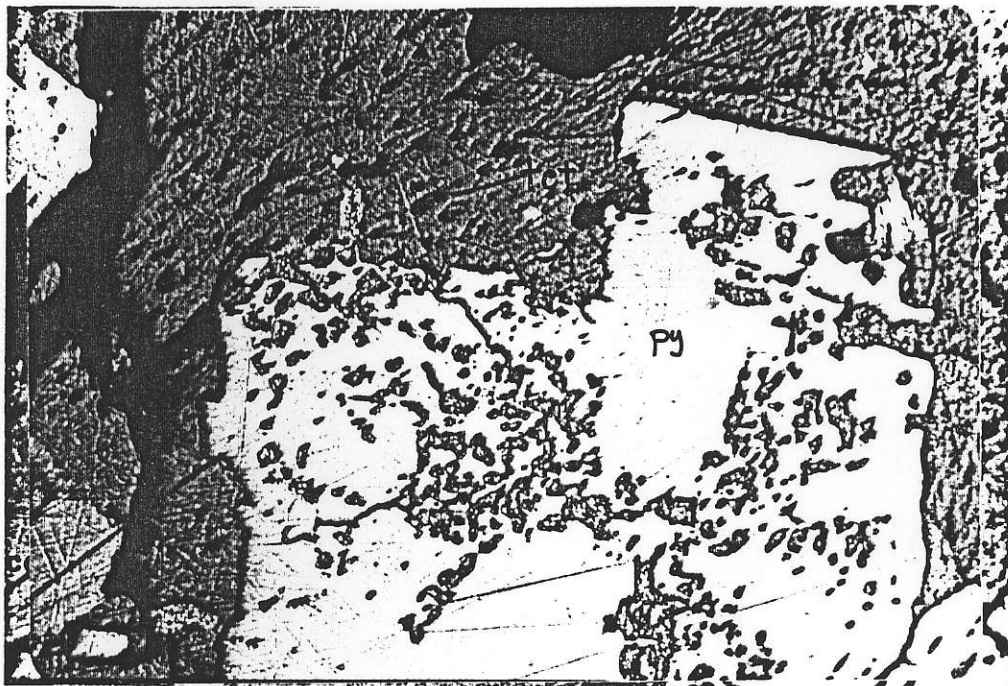


Fig. 10. Gold replacing pyrite and tetrahedrite.
Bear Vein. Mag: 500X

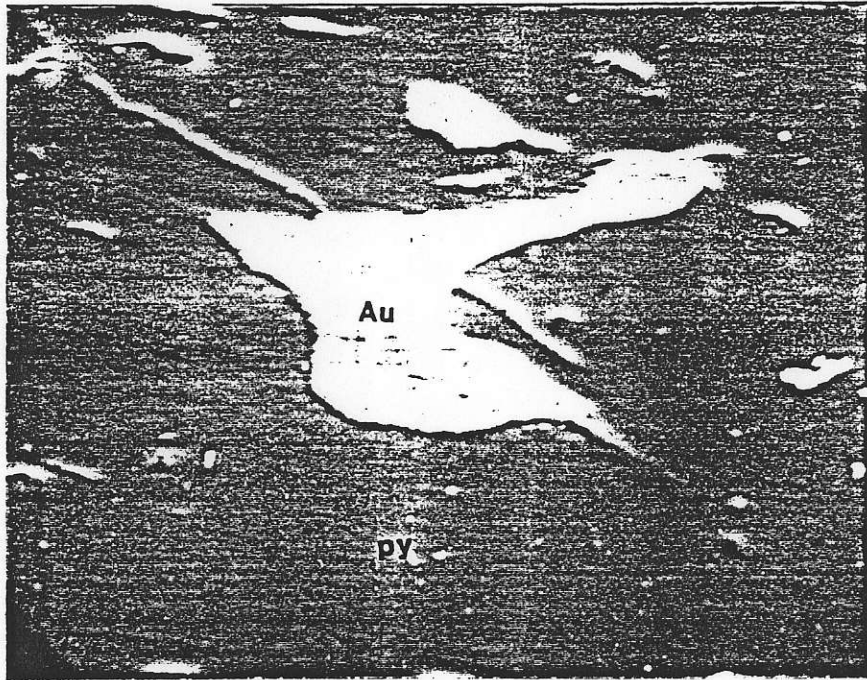


Fig. 11. SEM microphotograph of gold replacing pyrite. Jennie Vein. Mag: 2000X



Fig. 12. Photograph of listwanite, serpentine-carbonate zone

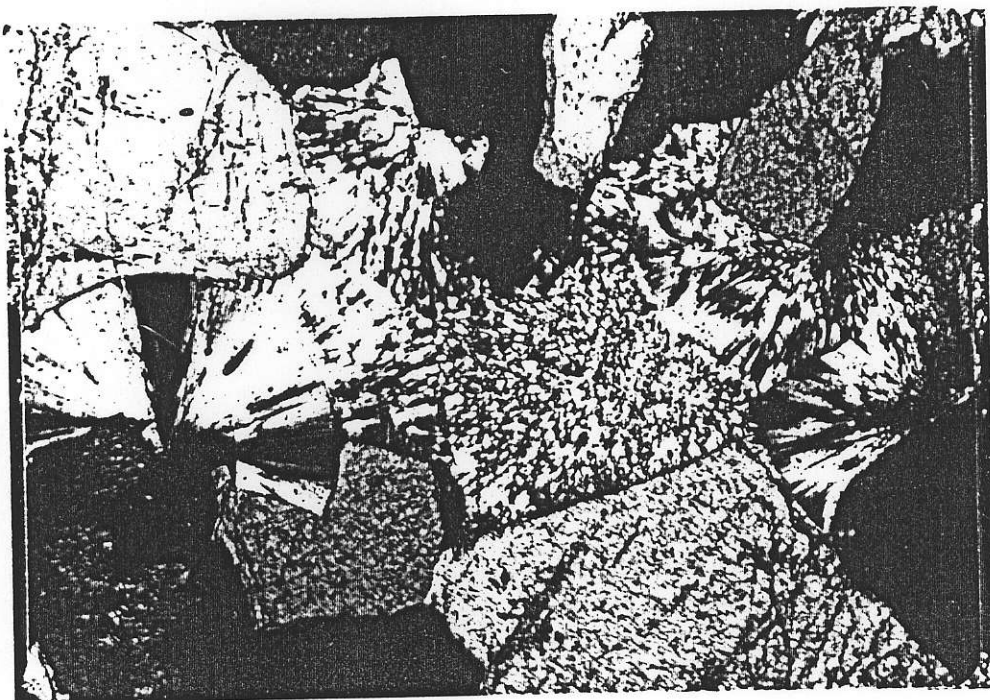


Fig. 13. Microphotograph of listwanite, serpentine-carbonate zone. Radial antigorite in magnesite. Magnification: 25X

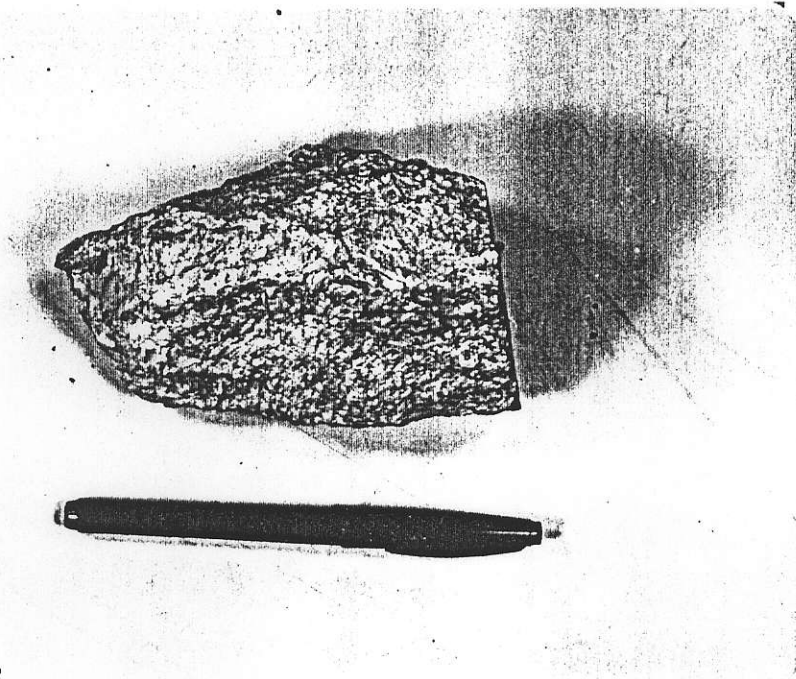


Fig. 14. Photograph of listwanite, talc-carbonate zone

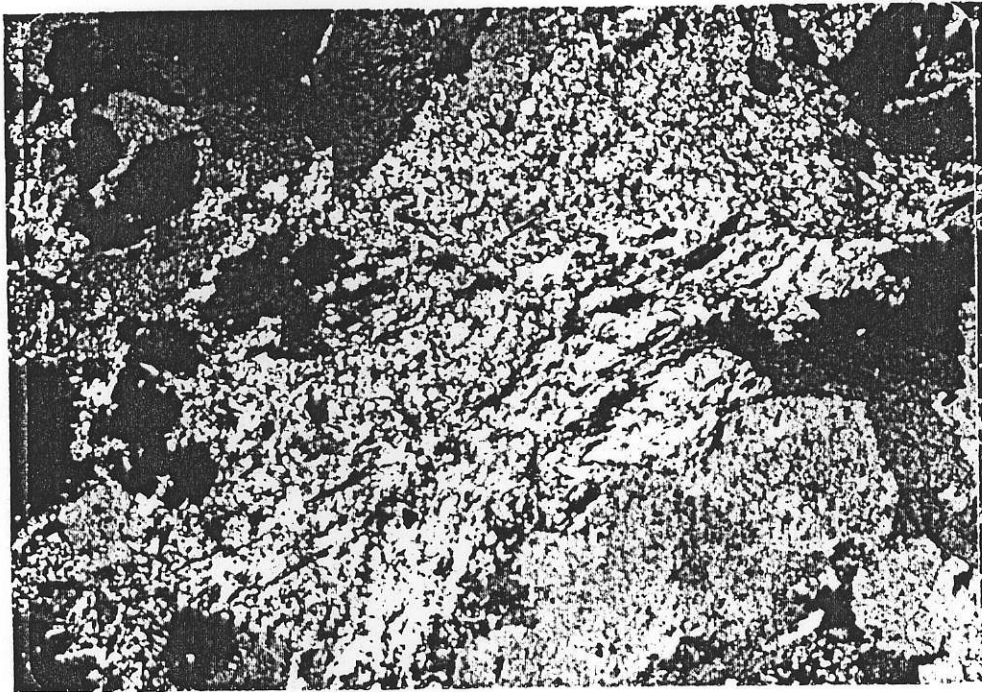


Fig. 15. Microphotograph of listwanite, talc-carbonate zone. Aggregate of feathery talc within carbonate. Mag: 25X

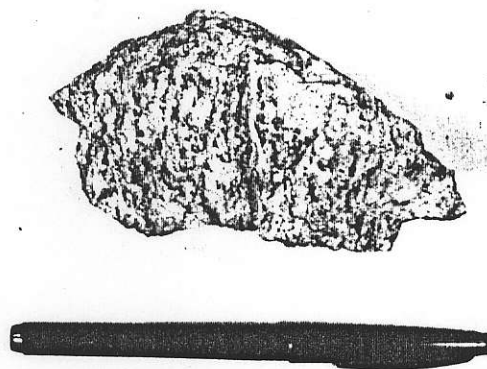


Fig. 16. Photograph of listwanite, quartz-carbonate zone

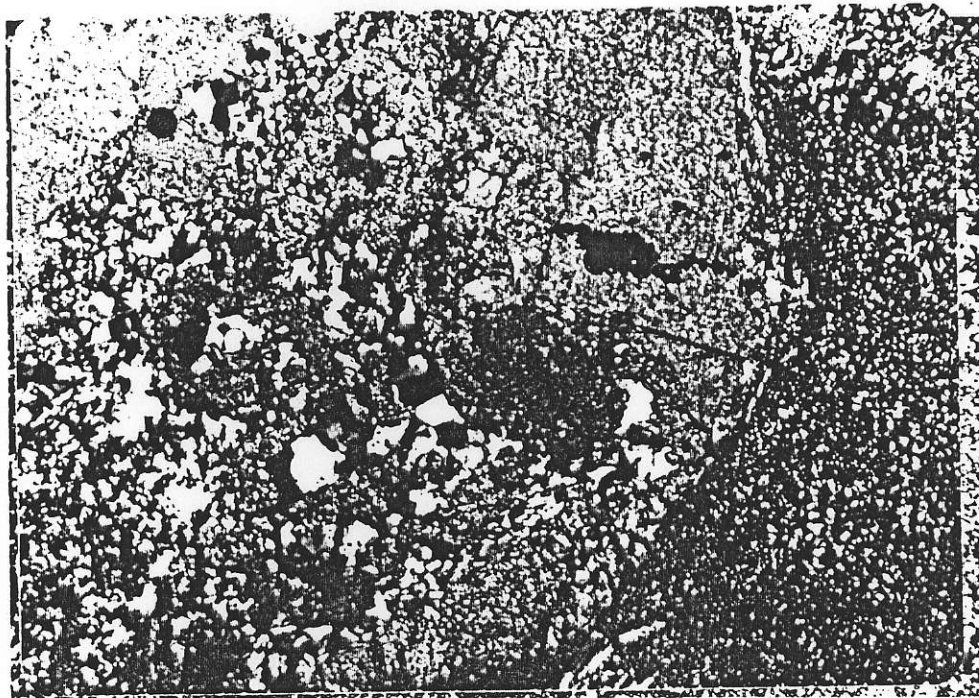


Fig. 17. Microphotograph of listwanite, quartz-carbonate zone.
Magnification : 25X

GEOCHEMISTRY OF LISTWANITES

Samples of listwanite at Erickson Mine were chemically analyzed to determine the chemical changes which took place during listwanite metasomatism.

Metasomatism commonly produces mineralogical zoning, each succeeding zone being of different mineral composition and separated from adjoining zones by sharp boundaries (Korzhinskii, 1970). Mineralogical zoning is prominent in the listwanites at Erickson and constitutes strong evidence for a metasomatic origin.

Metasomatism produces significant changes in rock chemistry attributable to reactions set up by introduction of material from external sources (Gary and others, 1976). This typically involves large amounts of fluid traversing permeable rocks with which it is out of equilibrium (Burt and Rose, 1979). Metasomatism is made possible by the presence of chemical and/or physical gradients. These gradients are most commonly present near magmatic intrusions or within highly fractured basaltic rocks emplaced along an oceanic rift at or just below the sea floor (Best, 1982).

Migration of elements during metasomatism occurs by diffusion or by infiltration. Diffusion involves the migration of material through stagnant pore fluids in response to activity gradients. Whereas during infiltration metasomatism, material is transported by fluid flow through permeable rock as a result of a pressure gradient (Burt and Rose, 1979). Although models for pure diffusion and pure infiltration have been formulated, in an actual ore depositing environment, both can occur simultaneously; fluids infiltrate along permeable channelways and material

diffuses into the wallrocks along grain boundaries (Burt and Rose, 1979).

I. Methods

At least three, largely concordant bodies of listwanite averaging about 30 meters in thickness occur within the volcanics at Erickson. These listwanite bodies are frequently crosscut by gold-quartz veins and consequently are well exposed within the mine workings. However, only the 1285 level East Drift includes the entire sequence of mineralogical zones. This area is therefore a useful "type-section" for studying the mineralogy, petrology and geochemistry of listwanites at Erickson (Figure 18). In order to identify the chemical changes during metasomatism, rock samples (labelled L-1 through L-16) were taken at five meter intervals throughout the length of the intersection. All samples were analyzed for the major elements, minor elements and the trace elements, cobalt, nickel, chromium, gold, hafnium, thorium and zirconium.

II. Results

A. Major and Minor Elements

Metasomatism commonly results in a change in rock volume. In order to determine the actual gains and losses that take place during metasomatism, the relationship between composition changes and volume changes must be known (Gresens, 1966). A composition-volume equation derived by Gresens (1966) directly relates compositional variations to volume changes which allows calculation of a unique solution for the chemical changes produced by metasomatism. In order to use this equation, it is necessary to know or infer the following data:

1. the chemical composition of both parent and product rocks
2. the densities of both parent and product rocks
3. the volume change or geochemical behavior of one component

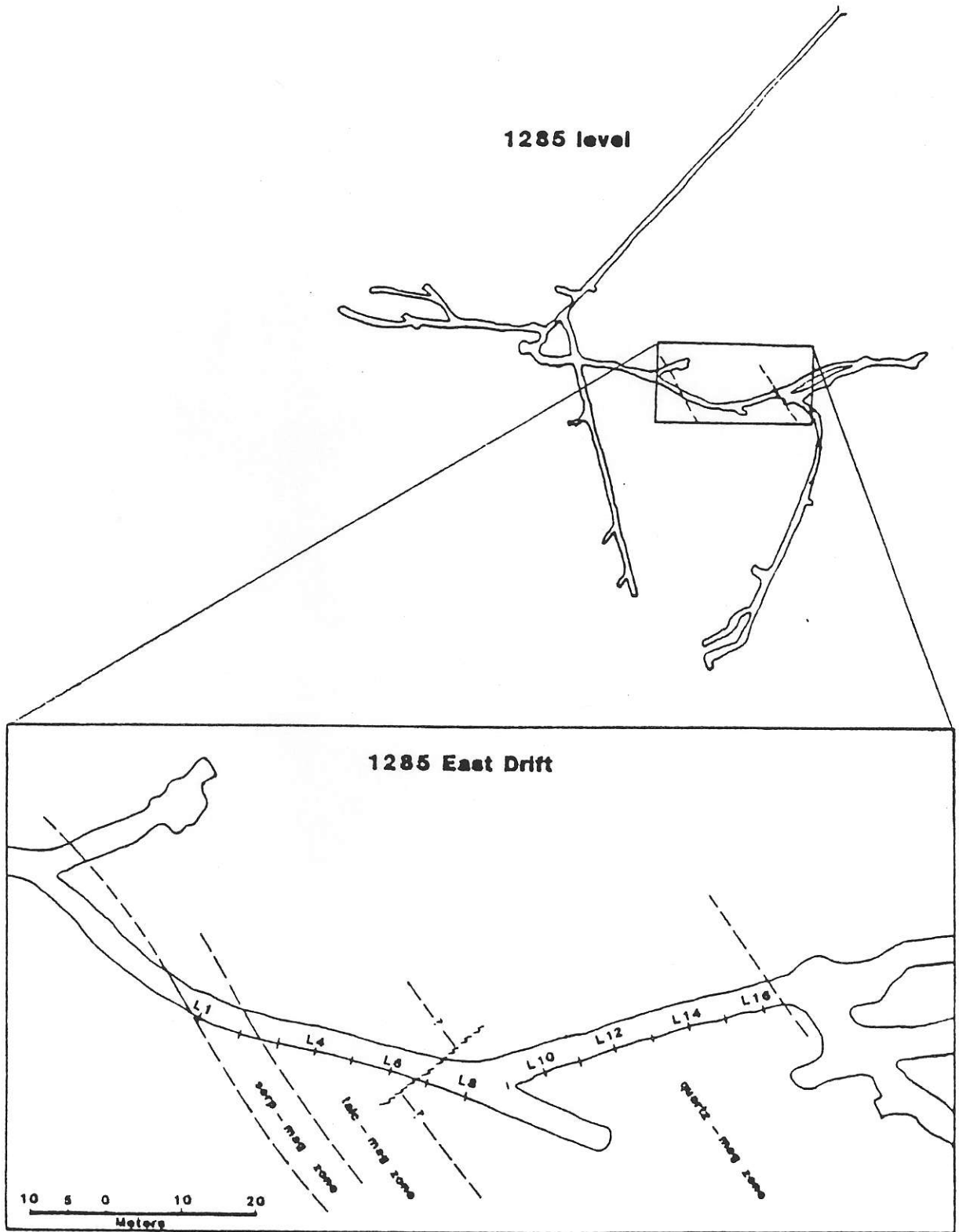


Fig. 18. Listwanite sample locations, L-1 through L-16, 1285 East Drift.

Using Babcock's (1973) modification of the notation, Gresen's composition-volume equation relates this data to chemical transfer in the following manner:

$$\Delta X_n = a \left[\left(K_v X_n^\beta \frac{\rho^\beta}{\rho^\alpha} \right) - X_n^\alpha \right] \quad (1)$$

where: ΔX_n = chemical transfer (in grams) of component n between phases A and B.

K_v = ratio between final and initial volume of rock

ρ^α = density of parent rock

ρ^β = density of product rock

The composition-volume equation can be used to yield considerable information on the chemical changes during metasomatism for samples L-1 through L-16. The methods used are similar to those described by Babcock (1973).

Most of the variables in the composition-volume equation (Eq. 1) can be measured or determined directly. For example, grams of component "n" in the product rock, i.e. X_n^β , were determined through chemical analysis. Because no parent rock material has been preserved in the mine area, a sample of serpentinite, which is presumed to represent unmetasomatized parent material, was selected from the Cassiar deposit nearby. Chemical analysis of the serpentinite provided the data for the variable X_n^α . The densities of both the presumed parent rock (ρ^α) and product rock (ρ^β) were measured on a balance scale modified to determine specific gravities. The number "100 grams" was substituted for the variable "a" in equation 1 in order to obtain ΔX_n in terms of weight percent. The equation, therefore, is solvable if a value can be determined or assumed for the volume ratio, K_v . The problems implicit in quantifying the volume change are apparent. Pseudomorphous replacement constitutes unequivocal

mineralogical evidence for volume-for-volume replacement, i.e. $K_v=1$, (Best, 1982). However, this was not observed in a thin-section study of these rocks. As an alternative, if a chemical component is known or assumed to have remained immobile during metasomatism, then the volume change which allows for this condition can be used to solve for the chemical changes of the other elements.

For example, Figure 19 indicates the weight percent gains and losses during metasomatism for samples L-1 through L-16. Volume ratios of 1.2, 1.0 and 0.8 were used in solving equation A which correspond to a 20 percent volume increase, no volume change, and a 20 percent volume decrease respectively. These values for K_v were selected arbitrarily as representing the broadest range of volume changes which are geologically reasonable. Chemical change (ΔX_n) for each element "n" was calculated for each individual sample L-1 through L-16 with results for each volume change plotted separately.

These diagrams illustrate the geochemical mobility of five major elements, calcium, iron, aluminum, silica and magnesium. Relative gains and losses for each element in terms of weight percent are plotted on the vertical scale for each individual sample L-1 through L-16 plotted on the horizontal scale. Several trends can be depicted. It is apparent that large amounts of MgO are extracted for all assumed volume changes. Increases in both CaO and Fe_2O_3 occur for all assumed volume changes although the magnitude of change is considerably less than that of MgO . The component SiO_2 shows extreme mobility and is extracted in significant amounts for decreases in volume. However, Al_2O_3 appears relatively immobile for all assumed volume changes. The volume at which this condition occurs can be calculated from equation 1 by rewriting the equation to solve for K_v and substituting "0" for the chemical change,

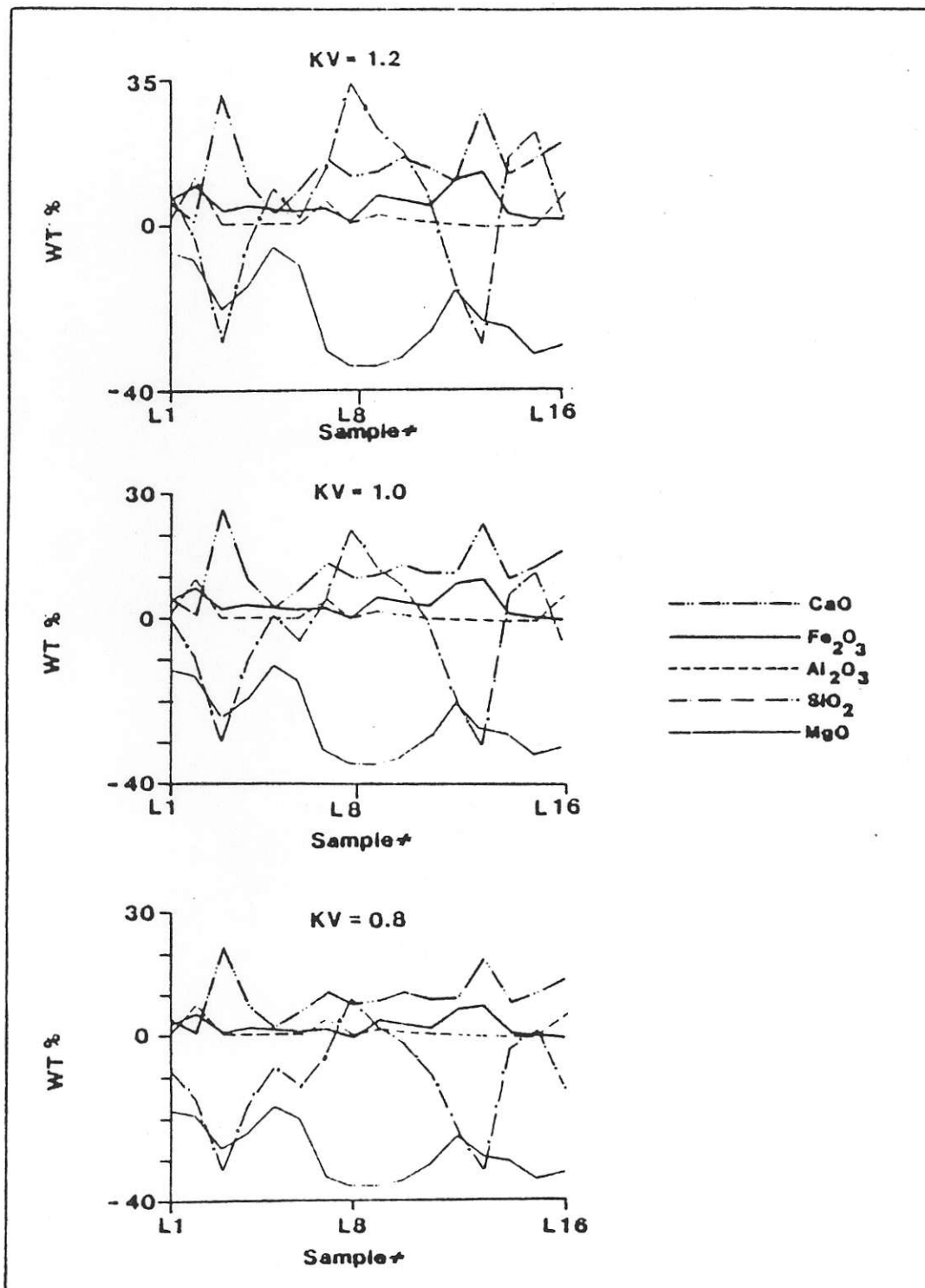


Fig. 19. Weight percent gains and losses of selected major elements during listwanite metasomatism.

ΔX_n . The value for K_v derived by solving the equation can then be substituted back into equation 1 and the chemical change for the remaining elements calculated.

For example, let Al_2O_3 be assumed to have remained constant during metasomatism and sample L-1 arbitrarily selected. If K_v is calculated for Al_2O_3 as described above, a value of 0.54 results which corresponds to a 46 percent decrease in volume, an unlikely situation. The minor elements appear even more isochemical in behavior (see Appendix I). Assuming both K_2O and Na_2O to have remained constant during metasomatism, K_v can be calculated for both these elements in the same manner as Al_2O_3 . A value of 0.66 results for both elements which corresponds to a volume decrease of 34.0 percent, still a large figure.

Figure 20 illustrates why these unexpectedly large volume changes are occurring from calculations assuming perfect isochemical behavior. In this volume-composition diagram, the five major elements depicted in Figure 19 are plotted. The straight lines illustrate the linear relation between composition and volume changes. An element whose behavior is isochemical during metasomatism will plot as a vertical line, as indicated. The slope for an element will approach the vertical as a condition of constant chemical composition is approached. If addition or subtraction of an element corresponds to a condition of 0 volume change, it will plot as a horizontal line at $K_v=1.0$.

The slope of Al_2O_3 is very steep indicating a condition approaching isochemical behavior. This condition is consistent with Figure 19. Of critical importance, however, is the fact that as a line approaches vertical, very small additions or subtractions result in large changes in volume. For example, Al_2O_3 shows approximate isochemical behavior

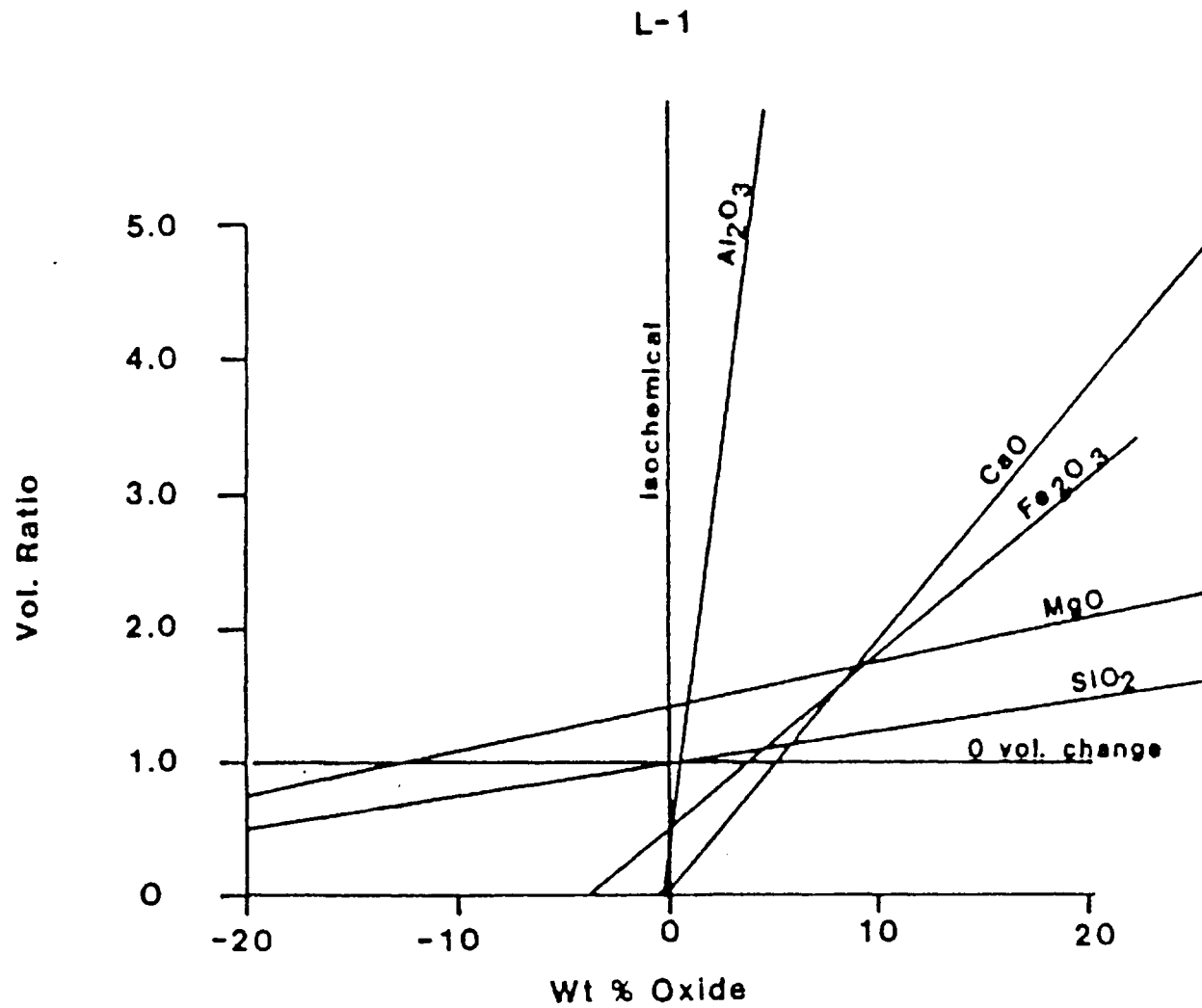


Fig. 20. Volume Ratio (K_v) versus compositional changes for conversion of parent rock, L-17, to L-1.

during metasomatism as indicated by the steep slope approaching vertical. However, a 0.5 weight percent increase in alumina during metasomatism, if "perfect" immobility is assumed for purposes of calculating K_v , results in an error exceeding a 50 percent volume change. The problem is compounded for elements with even steeper slopes. Therefore, false assumptions of "perfect" isochemical behavior compounded by analytical error cause extremely large errors in calculating volume ratios.

In summary, the volume change during listwanite metasomatism at Erickson cannot be calculated directly from the data by the method just described. However, the lack of any field evidence for a volume change during metasomatism supports an assumption of volume-for-volume replacement as being the most reasonable one for estimating gains and losses of the elements. Assuming no change in volume, i.e. $K_v=1.0$, the following chemical changes would have taken place during listwanitization:

1. Addition of CaO and FeO
2. Extraction of MgO and SiO_2
3. Al_2O_3 and the minor elements remained relatively immobile

B. Trace Elements

Chemical analyses for trace elements were undertaken to determine the parent rock composition of the listwanites (see Appendix I, p.86). Thirteen of the sixteen samples of listwanite contain no detectable concentration of any of the trace elements analyzed for, viz., nickel, cobalt, chromium, gold, hafnium, throrium and zirconium. However, three of the samples, L-1, L-5 and L-8 as well as the presumed parent rock, 0113, contain nearly identical concentrations of these elements. Furthermore, the concentrations of nickel, cobalt and chromium in these samples approximate worldwide averages for ultramafic rocks (Krasukopf,

1979). The similar amounts of these elements in both the presumed parent material, serpentized peridotite, and the samples of listwanite indicate a probable serpentized peridotite parent rock composition for the listwanite.

FLUID INCLUSION STUDIES

Constructing a chemical model of listwanite metasomatism involves plotting the equilibrium sulfide mineral assemblages of the Erickson lodes on phase diagrams from which estimates of the activities of various chemical components can be estimated. Because the value for the equilibrium constants for the chemical reactions used in constructing phase diagrams is temperature dependent, some representative temperature for the system must be estimated. Although the Erickson quartz lodes undoubtedly crystallized over a range of temperatures, analysis of fluid inclusions allows some single representative temperature to be estimated for purposes of constructing a model of the system.

Growth irregularities during crystallization entrap portions of the fluid medium from which the crystal is growing, resulting in a "fluid inclusion". These fluid inclusions average less than .01 mm in size (Roedder, 1976) and are common in all rocks and minerals (Evans, 1980). Considerable information, including the chemistry and density of the fluid and the temperature and pressure prevailing during entrapment, can be derived through microthermometric studies of fluid inclusions (Roedder, 1984).

I. Methods

Five gold-bearing quartz veins, the Jenny, Maura, Bear, Alison and Catlin were sampled at Erickson Mine. A total of thirty samples were selected from these veins in such a manner as to cover, as far as possible, the vertical and horizontal extent of each vein. The fluid inclusions in these veins were studied to determine the chemical composition and density of the hydrothermal fluid which transported and

deposited the gold, and the temperature and pressure of entrapment.

Each sample was cut into approximately 1 centimeter thick slabs which were examined under low magnification to select suitable material for cutting thin sections. The generation of quartz and presence or absence of mineralization was noted. If the thin section contained fluid inclusions of suitable size, a quartz chip about the size of a thumbnail was made and highly polished on both sides for maximum resolution. The quartz chip was then numbered and mounted temporarily on a glass slide.

A thorough search of the chip was undertaken to locate "primary" inclusions according to Roedder's (1976) criteria. The chip was sketched with the location of primary inclusions indicated. Fluid inclusion size, shape, type, occurrence and degree of fill was noted.

When mounted on the "heating-freezing" (microscope) stage, the chip is sandwiched between glass or silica windows within a cylindrical chamber which allows the passage of a hot or cold gas, either nitrogen or "air". The chip is connected to a thermocouple which registers the heat of the chip and indicates the temperature in degrees Celcius by digital display. A magnification of 512X is provided by 16X oculars and a special 32X objective with a very large free working distance (FWD). The chip is cooled by passing cold gaseous nitrogen through the chamber. Temperatures in excess of -100 C are attainable. Hot air passed through the chamber can heat the chip to temperatures approaching 600 C for those with a sense of adventure.

A. Observing Phase Changes

At room temperature, an inclusion may contain one fluid phase, both a liquid and a gas phase, two liquid phases, or a gas and two liquid phases. Also, one or more solids may be found in any of these types

(Hollister and others, 1981). The possible species present in significant amounts include H_2O , CO_2 , CO , H_2 , N_2 , CH_4 , H_2S , $NaCl$, KCl and $CaCl_2$ (Holloway, 1981). However, the most common species are H_2O , CO_2 and $NaCl$. "Microthermometry" is the technique for measuring the temperatures of phase transitions (Hollister, 1981). The temperature of these phase transitions indirectly indicates the chemical components of the system by reference to experimentally derived fluid phase equilibria.

All primary fluid inclusions observed in Erickson samples consisted of a single homogeneous liquid phase with a centrally located small vapor bubble which occupied about 30 percent by volume, of the inclusion. No solids or other liquid phases were observed.

1. Solid-Liquid Phase Transition

The fluid inclusions were cooled until the liquid was frozen. During cooling, the vapor bubble was seen to slowly contract until freezing of the liquid to ice below -30 degrees C. The freezing of the liquid phase was observed as a sudden crystallization which distorted the spherical shape of the vapor bubble, and as a sudden darkening of the inclusion, apparently caused by refraction of light by the ice crystals. The temperature at which this occurred, denoted "T_{min}", was recorded. The inclusion was then slowly heated at a rate of about one degree C per two minutes. At a temperature between -10 degrees C and -3 degrees C, the melting of the ice to a liquid, i.e. the solid-liquid phase transition, was observed. Resolution, except in rare cases, was insufficient to distinguish the initial melting, or eutectic melting (T_e) from the final melting or dissolution of ice, denoted T_m . At some temperature, the vapor bubble was observed to suddenly regain its spherical shape and the inclusion become lighter as the ice crystals melted. Several cooling runs

for each inclusion were made with the individual determinations averaged. If one particular determination varied greatly from others which were very closely grouped, an error in observation or metastability was assumed and the determination disregarded. Subsequent freezing runs on the same inclusion were made by rapid heating from T_{min} (usu. -30 C) to within 5 degrees of the initially observed melting temperature, T_e . The rate of 1 degree C per 2 minutes was then resumed to avoid metastability.

2. Vapor-Liquid Transition

As the inclusions were heated, the vapor bubble was observed to "homogenize" to the liquid, i.e. shrink and disappear in the liquid. The temperature at which this occurs, denoted T_h , is termed the "temperature of homogenization". As T_h was approached, the vapor bubble rapidly shrunk and darted quickly about the inclusion. At times, the vapor bubble was hidden by irregularities and reentrants within the inclusion. A slight cooling of the inclusion re-nucleated the vapor bubble and the inclusion was then reheated and the vapor-liquid transition temperature rechecked. Several heating runs for each inclusion were made with results averaged as in the freezing runs. Heating runs in excess of 480 degrees C failed to decrepitate any primary inclusions.

II. Results

Interpretation of fluid inclusion data requires obtaining an adequate number of measurements so that a pattern or trend is apparent when statistically studied. Depending upon the scale of the study and the complexity of the system, about 200 measurements are usually adequate. However, smaller numbers of measurements may be adequate for those ore deposit studies where a single generation of inclusions, all primary, is

available (Hollister and others, 1981).

Of the five quartz veins sampled at Erickson, only two veins, the Maura and the Alison, contained primary fluid inclusions suitable for study. Phase transitions, particularly the solid-liquid transition, are difficult to observe and require the resolution available only from those inclusions of a large enough size. The lack of suitable material may have been due, in part, to poor sampling technique of the Erickson lodes. Measurements were made on 45 primary fluid inclusions, 29 from the Maura vein and 16 from the Alison. All inclusions were located within the clear #2 and #3 generation quartz. A few measurements were made from fluid inclusions in sphalerite.

As a result of this study, the density and composition of the fluid, and the temperature and pressure conditions during entrapment can be reasonably estimated.

A. Chemical Composition

A fluid composition of moderately saline H_2O is indicated by measurements made on primary fluid inclusions found in the Erickson quartz lodes.

Dissolved salts, principally NaCl, depress the freezing point of H_2O . Therefore, measurement of the freezing point depression allows the salinity of the water to be indirectly determined.

The range of temperatures at which the solid-liquid phase transition was observed in samples of the Maura and Alison veins is illustrated in Figure 21. A freezing point depression of -6 degrees C is broadly representative of the system. The freezing point depression of H_2O with increasing salinity is illustrated in Figure 22. A horizontal line drawn from a -6 degree C freezing point depression on the vertical axis

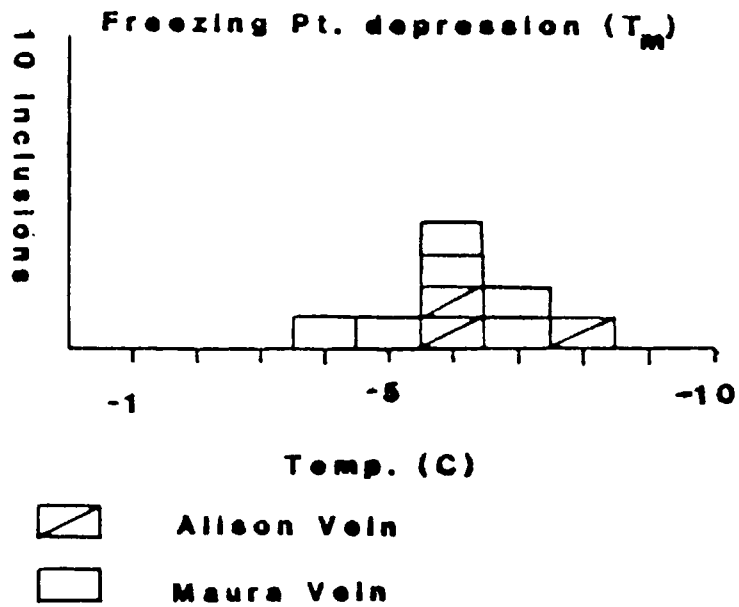


Fig. 21. Measurements of the H_2O solid - H_2O liquid transition temperature.

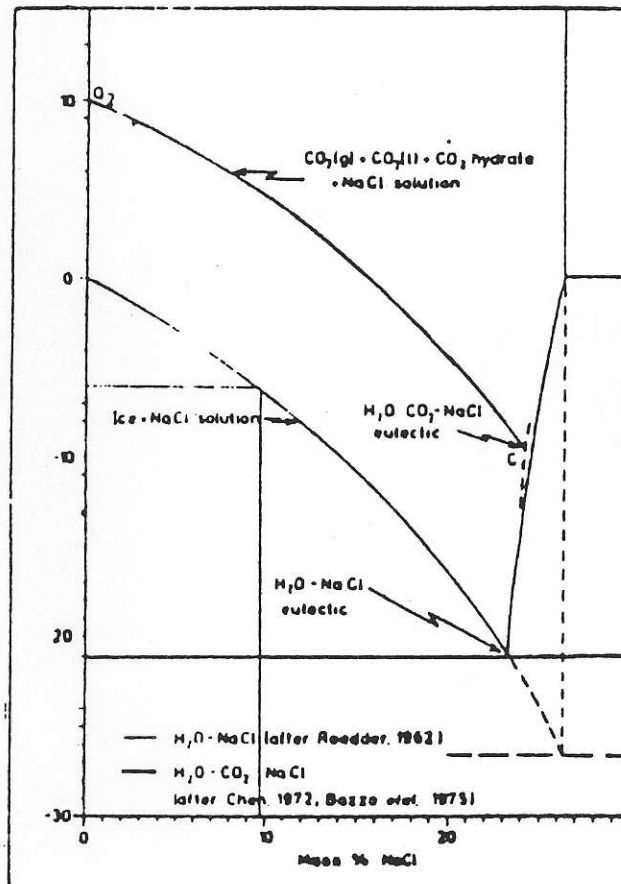


Fig.22 . The fusion temperature depression of ice by NaCl. (Modified after Collins, 1979)

correlates with an approximate 10 weight percent NaCl solution, as indicated in the figure.

B. Fluid Temperature, Pressure and Density

Primary fluid inclusions are assumed to contain portions of the original fluids whose composition and density have remained unchanged since entrapment. If a single homogeneous liquid phase is entrapped at some pressure (P_t) and temperature (T_t), (point A, Figure 23), the liquid will cool along a path of constant density called an "isochore". When the liquid cools to the temperature at which the isochore intersects the "boiling curve", a vapor bubble will nucleate and grow as temperatures continue to fall. The "boiling curve" or "two phase co-existence curve" is a region of pressure and temperature where the liquid is in equilibrium with its vapor. The temperature of the isochore-boiling curve intersection is the homogenization temperature, T_h . At this temperature, the vapor bubble can be observed to homogenize to the liquid. However, to determine the temperature of entrapment, a temperature correction must be made by an independent pressure correction, since P_t uniquely determines T_t . The load pressure or hydrostatic pressure can often be estimated from geologic evidence. An appropriate geobarometer may also allow estimation of the pressure of entrapment.

The constancy of the fluid/vapor ratio of the fluid inclusions in samples of Erickson ore indicate that a single homogeneous liquid phase was entrapped. Diversity in the fluid/vapor ratio is indicative of boiling. Only if a boiling fluid is entrapped is $T_t = T_h$.

Figure 24 shows the range of temperatures at which the water vapor bubble was observed to homogenize to the liquid in the primary fluid inclusions of both the Maura and Alison veins. The lack of a clear trend

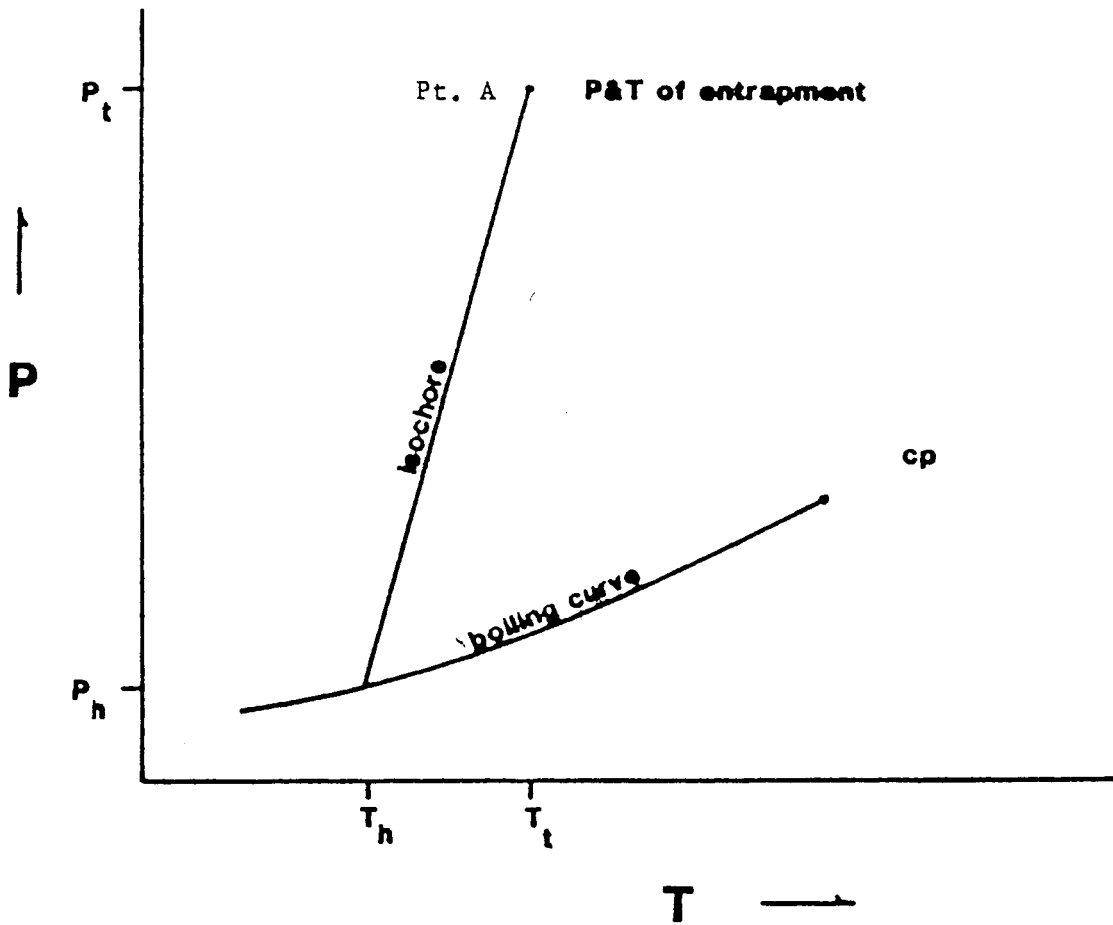


Fig. 23. A fluid entrapped at point A cools along a path of constant density, an isochore. At temperature T_h , a vapor bubble nucleates. The vapor bubble grows as cooling continues down the boiling curve.

Fluid Inclusion vapor-liquid (H₂O) homog. Temperatures

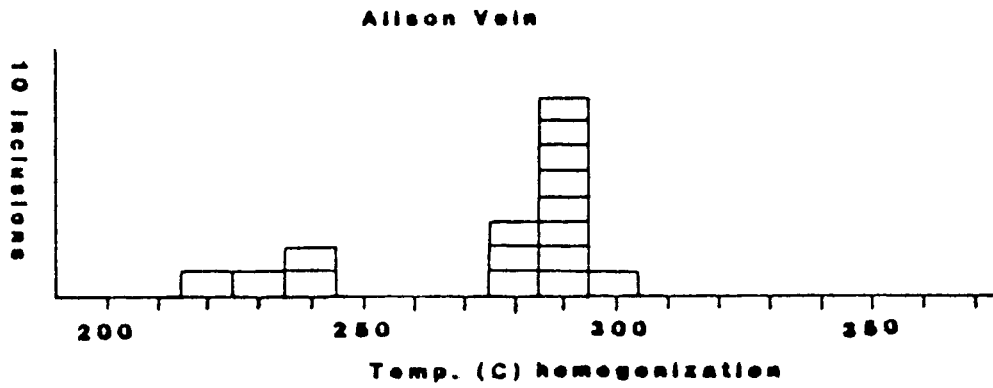
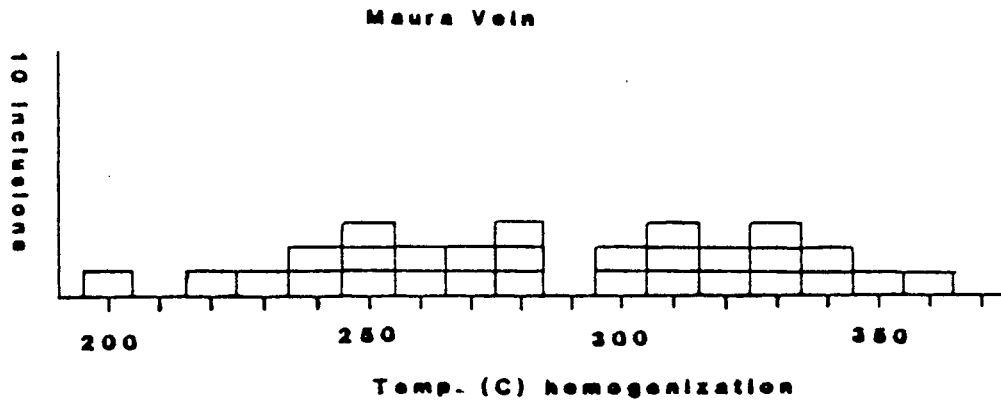


Fig. 24. Measurements of the H₂O liquid - H₂O vapor transition temperature.

from which some T_h can be unambiguously selected as representative of the system, can be attributed to two main factors:

1. Ore deposits commonly form, not at a single temperature, but over a temperature interval, sometimes as wide as 50-500 degrees C (Krauskopf, 1979).
2. An insufficient number of determinations were made for a clear trend to emerge.

On the basis of a weak trend which is apparent when the diagrams in Figure 24 are superimposed, a temperature of 285 degrees C is selected for T_h . The arbitrariness of such a selection is conceded. But since a selection of some single representative T_h must be made for purposes of calculation, 285 degrees C seems the most reasonable one.

The necessity of determining the true entrapment temperature by an independent pressure correction is an additional complication. Since gold-bearing quartz veins at Erickson occur throughout a wide range of elevations, the estimation of a specific load pressure is not possible (Panteleyev, personal communication, 1984). However, a moderate depth of burial is indicated by the vein mineralogy and structure, the lower greenschist metamorphic grade of the host rocks and the extensive alteration halos of the quartz lodes. Since most deposits are formed at modest pressure (Krauskopf, 1979), and vein structure and mineralogy indicate a moderate temperature/pressure of formation, a load pressure of 625 atms is arbitrarily assumed to be broadly representative. As Figure 25 indicates, a load pressure of 625 atms uniquely determines a 350 degree C temperature of entrapment.

It is assumed therefore, that 350 degrees C falls within the range of temperatures at which the Erickson lodes crystallized, and can be assumed broadly representative for purposes of constructing a model of the system.

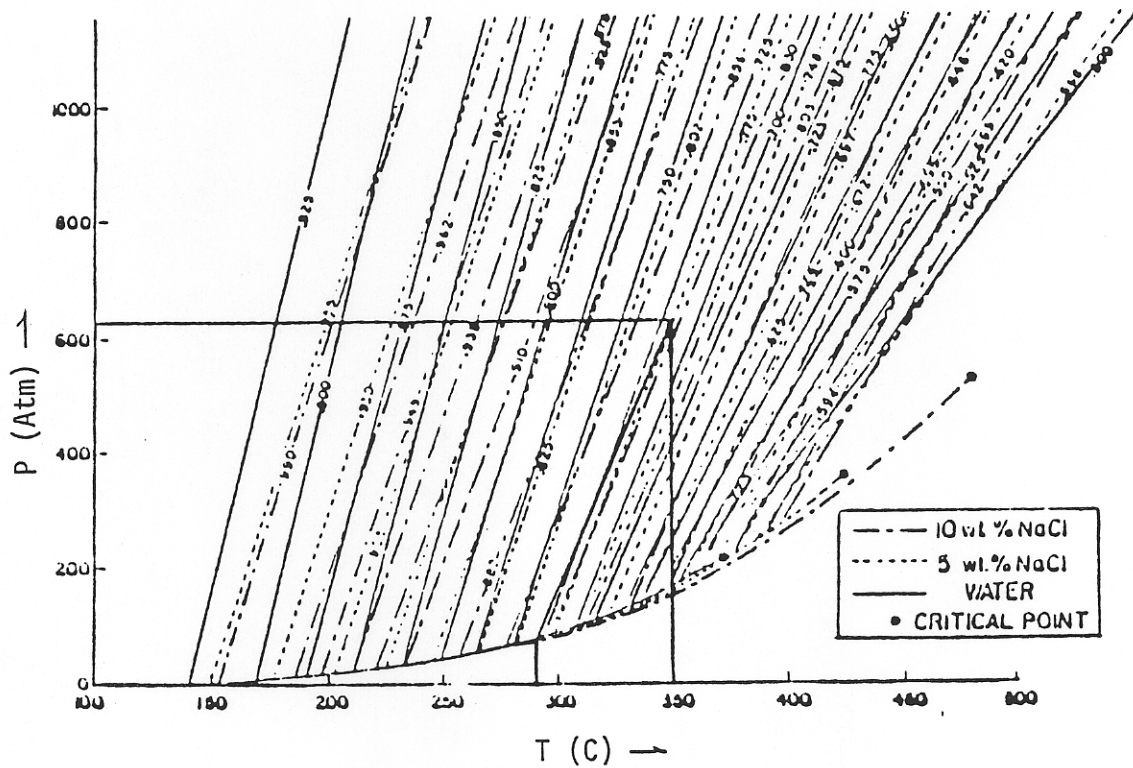


Fig. 25. Vapor pressure curves for water, 5 wt percent NaCl and 10 wt percent NaCl solutions. Determination of T_1 (285 C) locates the isochore along which entrapment occurred. A pressure correction of 625 atm uniquely determines T_t , the temperature of entrapment - 350 C (After Roedder, 1984)

DISCUSSION

A model illustrating how listwanites affect gold mineralization can be constructed from thermodynamic calculations based upon mineralogical, geochemical and fluid inclusion studies of Erickson rocks. It is proposed that hydrothermal fluids carrying gold in solution migrated up steeply dipping faults which crosscut bodies of serpentized peridotite. The fluids permeated and metasomatically altered these rocks producing the zoned silica-carbonate metasomatites termed "listwanite". Gold solubility was affected during metasomatism causing gold to migrate down activity gradients and precipitate out in adjacent quartz lodes.

In order to construct this model, the following data must be known or inferred:

1. the chemical composition of the ore solution
2. the chemical composition of the listwanite parent rock
3. the chemical composition of a fluid in equilibrium with the parent rock
4. the gold-transport complex
5. the chemical components which affect solubility of the gold complex

With the above information, the activity gradients which would exist across a listwanite body during fluid mixing can be calculated and the behavior of gold in these gradients determined. The relative affect of each chemical component on gold solubility can be calculated and the mechanism causing gold precipitation identified. The experimentally derived values for $\log K$ utilized in the calculations are listed in Table I.

TABLE I. Selected Equilibrium Constants (350 C)

<u>Reactions</u>	<u>Log K</u>	<u>Reference</u>
$\text{H}_2\text{S} + 2\text{O}_2 = \text{SO}_4^{2-} + 2\text{H}^+$	+41.0	A
$\text{H}^+ + \text{HSO}_4^- = \text{H}_2\text{S} + 2\text{O}_2$	-50.2	A
$\text{HS}^- + 2\text{O}_2 = \text{SO}_4^{2-} + \text{H}^+$	+50.6 (extrap)	A
$\text{HSO}_4^- = \text{SO}_4^{2-} + \text{H}^+$	-9.2	A
$\text{HS}^- = \text{H}^+ + \text{S}^{2-}$	-9.95	A
$\text{H}_2\text{S} = \text{H}^+ + \text{HS}^-$	-8.69	A
$\text{H}_2\text{CO}_3 = \text{H}^+ + \text{HCO}_3^-$	-10.2	A
$\text{HCO}_3^- = \text{H}^+ + \text{CO}_3^{2-}$	-12.4	A
$2\text{FeS} + \text{S}_2 = 2\text{FeS}_2$	+8.76	A
$5\text{CuFeS}_2 + \text{S}_2 = 4\text{FeS}_2 + \text{Cu}_5\text{FeS}_4$	+5.14	A
$3\text{FeS}_2 + 2\text{O}_2 = \text{Fe}_3\text{O}_4 + 3\text{S}_2$	+32.36	A
$4\text{Cu} + \text{S}_2 = 2\text{Cu}_2\text{S}$	-18.80	A
$\text{Cu}_2\text{S} + 1/2 \text{S}_2 = 2\text{CuS}$	+1.50	B
$3\text{KAlSi}_3\text{O}_8 + 2\text{H}^+ = \text{KAl}_3\text{Si}_3\text{O}_{10}(\text{OH})_2 + 6\text{SiO}_2 + 2\text{K}^+$	+7.8 (extrap)	A
$2\text{KAl}_3\text{Si}_3\text{O}_{10}(\text{OH})_2 + 2\text{H}^+ + 3\text{H}_2\text{O} = 3\text{Al}_2\text{Si}_2\text{O}_5(\text{OH})_4 + 2\text{K}^+$	+4.9 (extrap)	A
$\text{KAlSi}_3\text{O}_8 + \text{Na}^+ = \text{NaAlSi}_3\text{O}_8 + \text{K}^+$	-0.65	D
$\text{Au} + 2\text{H}_2\text{S} + \text{HS}^- = \text{Au}(\text{HS})_2^- + 1/2 \text{H}_2$	-1.08	B
$\text{H}_2\text{O} = \text{H}_2 + 1/2 \text{O}_2$	-18.0	A
$\text{Au} + 2\text{H}_2\text{S} + 1/4\text{O}_2 = 1/2\text{H}_2\text{O} + \text{H}^+ + \text{Au}(\text{HS})_2^-$	+7.95 (extrap)	C
$\text{Au} + 2\text{Cl}^- = \text{AuCl}_2^-$	+ 6.2	C
$\text{C (graphite)} + \text{O}_2 = \text{CO}_2$	+33.08	A

Table I. Continued

$C \text{ (graphite)} + O_2 + H_2O = H_2CO_3$	+31.48	A
$H_2CO_3 + H_2O = CH_4 + 2O_2$	-63.28	A
$Fe + 1/2 O_2 = FeO \text{ (var. Wustite)}$	+18.84	E
$1/2 Fe_3O_4 + 1.5 Fe + O_2$	-37.2	E

A.) Crerar and Barnes, 1976; B.) Barnes, 1979; C.) Casadevall and Ohmoto, 1977; D.) Hegelson, 1969; E.) Robie and Waldbaum, 1968.

I. Determining The Chemistry of the Ore Solution

Fluid inclusion studies indicate that a 10 weight percent NaCl-H₂O solution was entrapped at an approximate temperature of 350 degrees C and under a pressure in excess of 625 atms. This data, in conjunction with mineralogical evidence, allows estimation of other chemical parameters including oxygen fugacity, pH, aK⁺, and total carbon and sulfur of the ore solution by construction of an fO₂-pH chemical diagram.

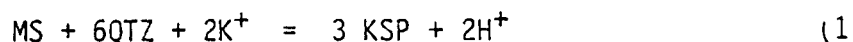
A. Construction of an fO₂ -pH diagram

Figure 26 shows that the pH and oxygen fugacity of the hydrothermal fluid are constrained by the stable coexistence of certain mineral phases. Because the value of the equilibrium constants for the relevant reactions are temperature dependent, the diagram is constructed for a temperature of 350 degrees C.

1. Determination of pH

At Erickson, wall rock alteration studies indicate that sericite was in equilibrium with the ore solution (Sketchley, personal communication, 1984). Since sericite is stable only over a small range of pH, calculation of its stability range indicates the approximate pH of the ore solution.

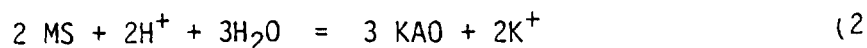
With increasing pH, sericite alters to orthoclase by the reaction:



Solving this equation for pH:

$$pH = -\log K/2 - \log [K^+] \quad (1a)$$

As pH decreases, sericite alters to kaolinite according to the reaction:



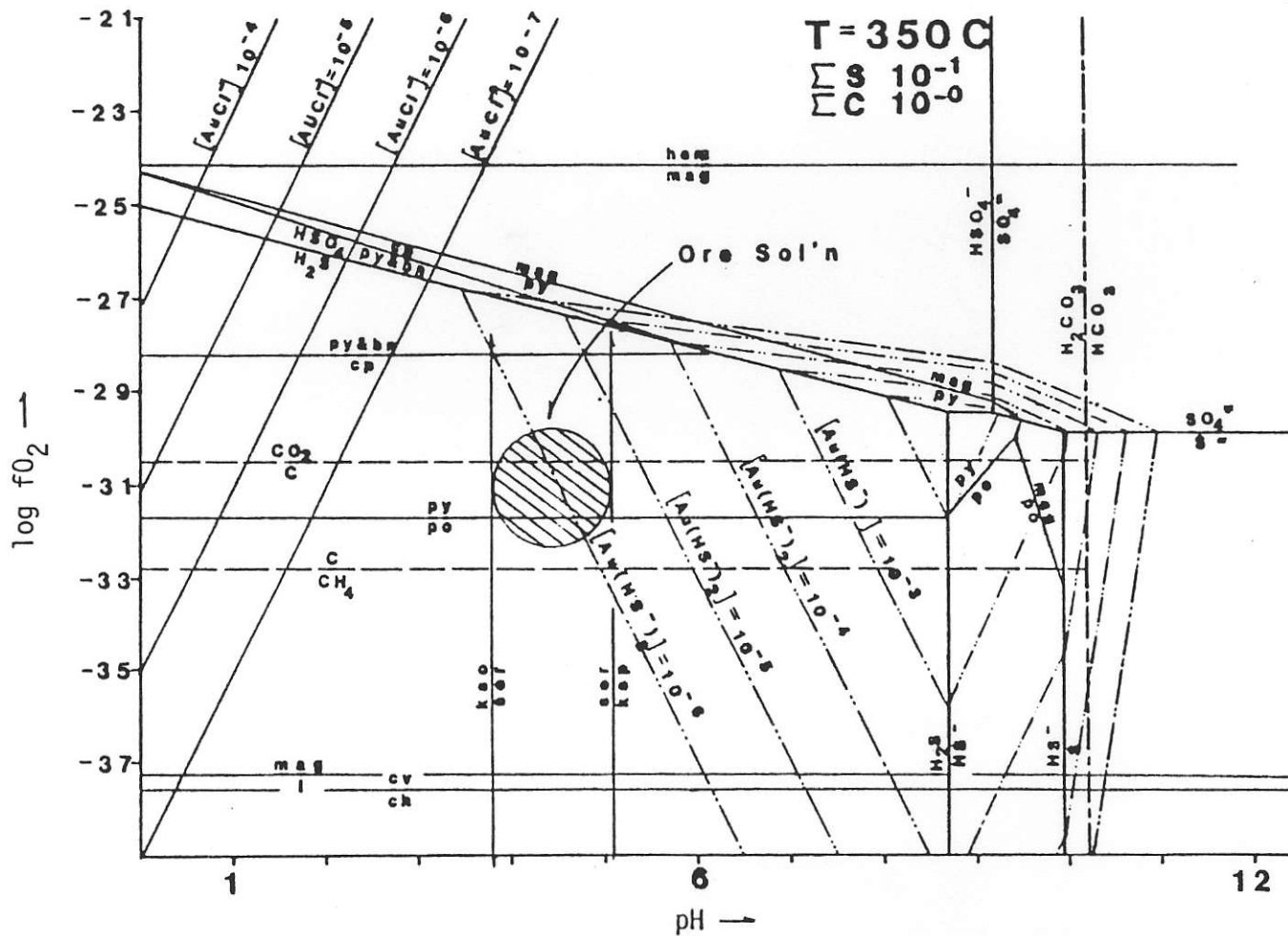


Fig.26. The stabilities of minerals from Erickson Mine at 350 degrees C with gold solubility as chloride and bisulfide complex plotted.

Solving for pH:

$$\text{pH} = \log K/2 - \log [K^+] \quad (2a)$$

Log K for reactions 1a and 2a are -7.8 and +4.9 respectively (Cerar and Barnes, 1978). In order to solve for pH however, $\log [K^+]$ must be estimated. A value for the activity of potassium (a_{K^+}) can be calculated indirectly from the salinity as determined from fluid inclusion measurements. However, to use this method, it must be assumed that, at depth, the ore solution was in contact with both albite and alkali feldspar which were in equilibrium according to the reaction:



Log K for this reaction is -0.65 as extrapolated from Hegelson (1969). Solving for log K:

$$\log K = \log [K^+] - \log [\text{Na}^+] \quad (3a)$$

Since log K is known, determining $\log \text{Na}^+$ will allow calculation of $\log [K^+]$.

The activity of sodium (a_{Na^+}) is related to the concentration of sodium in moles per liter (m_{NaCl}) by the equation:

$$a_{\text{Na}^+} = m_{\text{NaCl}} \times \lambda_{\text{NaCl}} \quad (4)$$

where λ_{NaCl} is the stoichiometric mean activity coefficient of NaCl. A value of 0.125 is extrapolated from Hegelson (1969). A 10 weight percent NaCl solution is equivalent to a 1.7 molar solution (m_{NaCl}). Substituting these values back into equation 4:

$$a_{\text{Na}^+} = (1.7) (0.125) = 0.213 \quad (5)$$

Substituting this value back into equation 3a and solving for $\log [K^+]$:

$$\log [K^+] = (-0.65) + (-.672) = -1.32 \quad (6)$$

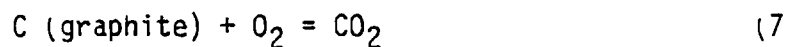
Substituting this value for $\log [K^+]$ back into equations 1a and 2a, the pH for these two equations are calculated to be 5.22 and 3.77 respectively.

Therefore, the pH of the ore solution lies within the general area of 3.77 and 5.22 as determined by the stability of sericite.

2. Determination of fO_2 , total carbon and total sulfur

As illustrated by Figure 26, the oxygen fugacity of the ore solution is constrained by the presence of pyrite and absence of pyrrhotite, and by the presence of graphite and absence of CO_2 in the quartz lodes.

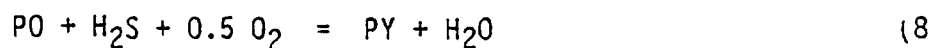
Graphite oxidizes to CO_2 by the reaction:



Solving for log K:

$$\log K = \log [CO_2] - \log [O_2] \quad (7a)$$

The presence of graphite and absence of CO_2 therefore establishes an upper limit to the oxygen content of the system. With decreasing oxygen content, pyrite reduces to pyrrhotite according to the reaction:



Log K for this reaction is :

$$\log K = -2 \log [H_2S] - \log [O_2] \quad (8a)$$

In order to solve equations 7a and 8a for $\log [O_2]$, it is necessary to estimate ΣC and ΣS for the system. An $fO_2 - T$ diagram (Figure 27) can be used to determine the minimum amounts of carbon and sulfur.

This diagram shows the $fO_2 - T$ stability fields for pyrite and graphite for various assumed values of ΣS and ΣC at periodic temperature intervals from 200 degrees C to 350 degrees C. The lines between mineral phases are determined in the same manner as the kaolinite - sericite - orthoclase lines. At some temperature, values for ΣS and ΣC are arbitrarily assumed and the equation solved for oxygen fugacity.

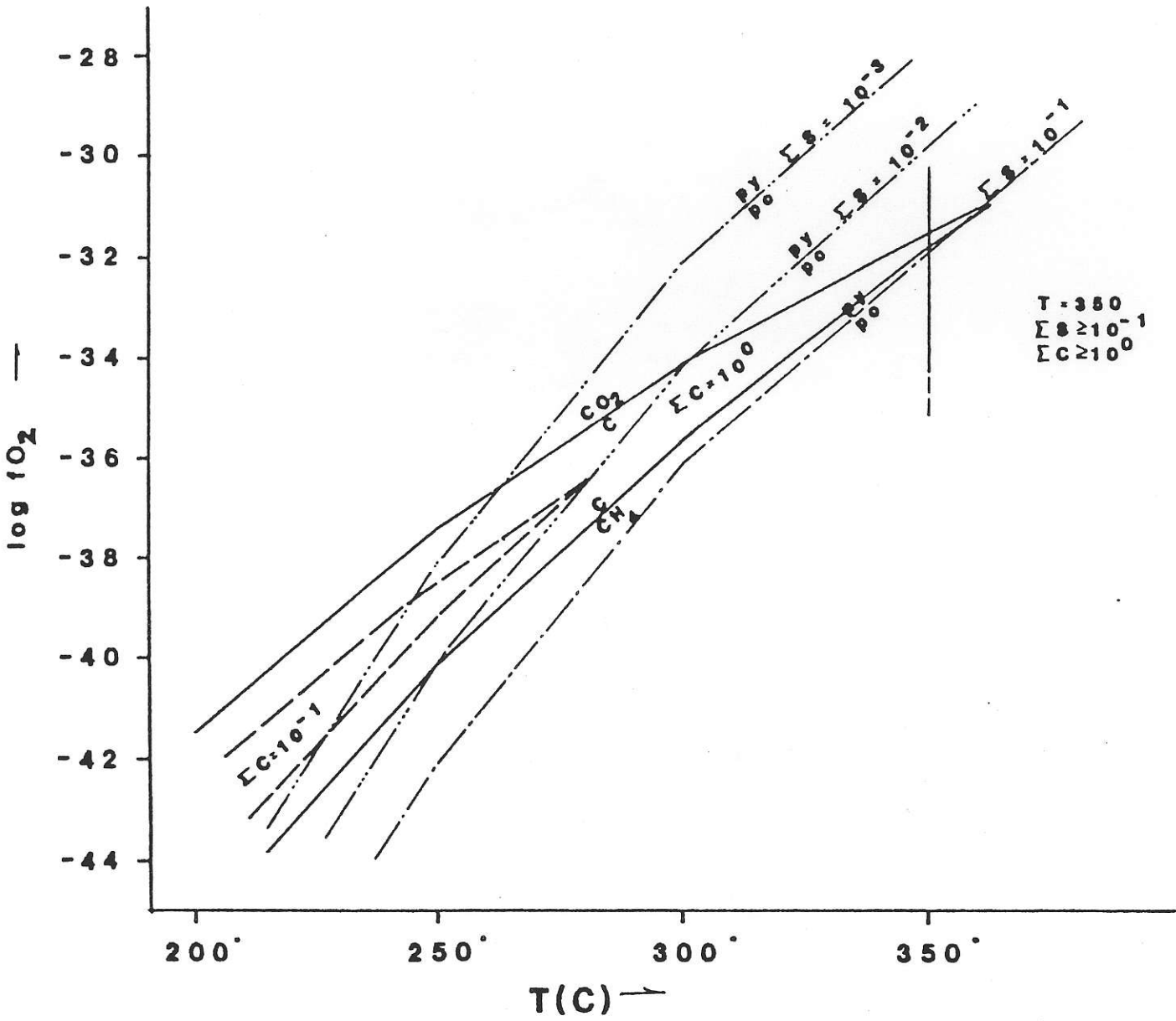
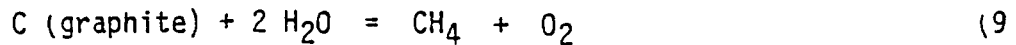


Fig. 27. Log f_{O_2} - T diagram showing the stability fields of pyrite and graphite for various assumed values of ΣS and ΣC .

For example, to locate the graphite-methane line at a temperature of 200 degrees C, a value of 10^{-1} is assumed for ΣC . Graphite reduces to methane by the reaction:



Log K for this reaction is -45.38 (Cerar and Barnes, 1976). The equilibrium constant is:

$$\log K = [CH_4] [CO_2] / 1 \quad (9a)$$

Solving for log O_2 :

$$\log [O_2] = \log K - \log [CH_4] \quad (9b)$$

Substituting values for log K and $[CH_4]$:

$$\log [O_2] = -45.38 - (-1) = -44.38 \quad (9c)$$

Therefore, at a temperature of 200 C and $C = 10^{-1}$, graphite reduces to methane at $\log fO_2 = -44.38$.

At a temperature of 350 degrees C, the stable coexistence of pyrite and graphite is possible only if ΣC equals or exceeds 10^0 and ΣS equals or exceeds 10^{-1} .

Using these values for solving equations 7a and 8a, the oxygen fugacity of the ore solution lies within the $\log fO_2$ range of -30.48 to -31.76 as indicated in the diagram.

II. Determining the Parent Rock Composition of the Listwanite

The probable parent rock composition of the listwanites at Erickson can be estimated from the crustal setting, mineralogy and trace element geochemistry of these rocks.

A. Crustal Setting

A thorough study of the literature by the writer corroborates Kashkai and Allakhverdiev's (1971, p.3) statement that listwanites are "genetically confined to" and "are possible only within the confines of the ultrabasic formation and its haloes". In particular, listwanites are associated exclusively with "Alpine-type" peridotites.

There are five separate lithological types of ultramafic rocks: 1. lamprophyres, 2. melilite-rich rocks, 3. carbonatites, 4. kimberlites, and 5. peridotites and allied rocks (Williams and others, 1982). However, only peridotites are of significant total volume and global extent (Chidester and Cady, 1972). Listwanites are restricted in occurrence to peridotites and allied rocks. Peridotites typically occur in two independent tectonic-geographical situations: 1. Massive basal cumulate layers in stratified basic continental plutons, e.g. Bushveld Complex, South Africa, and 2. Allocthonous bodies in folded orogenic mountain chains, i.e. "Alpine-type" peridotites. Listwanites are restricted to this later category.

The listwanites at Erickson Mine are hosted within an assemblage of volcanics and sediments of oceanic affinity thrust onto a miogeoclinal wedge of continental sediments autochthonous to the North American Craton. The listwanites occur within a linear belt of ultramafic rocks termed the "McDame ultramafic belt" by Gabrielse (1963, p.63). The crustal setting

of the listwanites at Erickson is in close agreement with other listwanite occurrences reported in the literature which indicates a probable Alpine-type peridotite parent rock.

B. Listwanite Mineralogy

Ultramafic rocks are characterized chemically as having a low silica and high magnesium content with commonly significant amounts of chromium. Being composed dominantly of the high temperature silicates, olivine, pyroxene and chromite, they are out of equilibrium within the upper crust and subject to deuteric and hydrothermal alteration. This alteration involves the interaction between high temperature silicates and introduced water producing low temperature hydrous silicates. Common alteration products include, serpentine, talc, brucite, amphiboles, sphene, hydrated Ca-Al silicates, chlorite, clays, calcite, albite, Fe-oxides, native metals and low-sulfur sulfides (Moody, 1976).

The listwanites at Erickson are composed of the typical alteration products of ultramafic rocks, viz. talc, serpentine, magnesite and chrome mica. As shown in Figure 28, at a temperature of 350 degrees C, the alteration mineral assemblages observed at Erickson can be produced by altering a serpentinite or serpentinized ultramafic rock with a CO₂-rich fluid. This represents strong evidence for a serpentinite or serpentinized ultramafic parent rock composition. Trace amounts of minerals containing chromium, cobalt and nickel, such as kammererite (chrome chlorite), numite (nickel chlorite), spinel, chromite and ferro-spinel are indicated by X-ray diffraction and constitute additional evidence for an ultramafic source rock.

C. Listwanite Trace Element Geochemistry

In samples of Erickson listwanite analyzed for trace elements, nickel

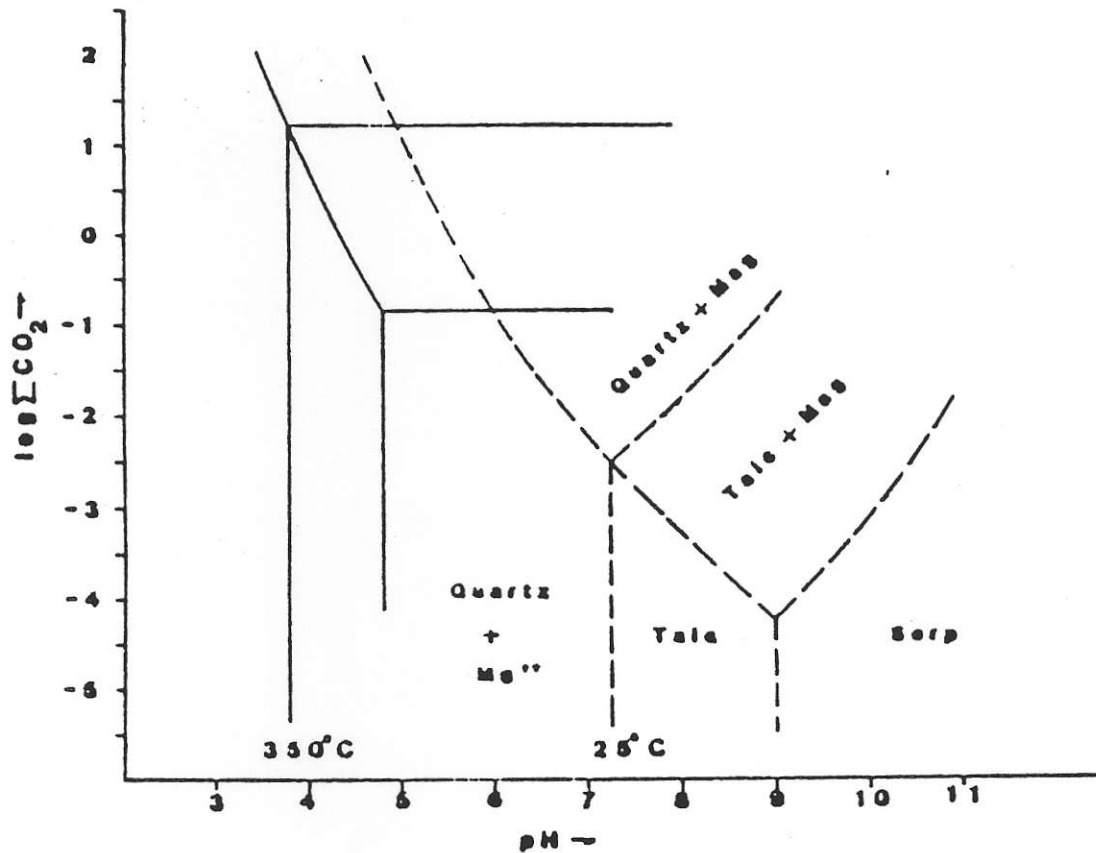


Fig. 28. Regions of stability of some compounds in the system MgO - SiO₂ - CO₂ - H₂O under standard and hydrothermal conditions (Modified after Shcherban' and Borovikova, 1969)

III. Determination of the Gold Transport Complex

The solubilities of ore minerals as simple ions, has long been recongized as inadequate to transport ore (Barnes, 1979). Under hydrothermal conditions, ore chemistries are restricted by both the limited number of dominant ore minerals and by the few ligands that are present in sufficient quantities to associate with metals in complexes (Barnes, 1979). In ore solutions, chloride and sulfide complexes are dominant, but antimonothio or arsenothio complexes may be locally prominant where indicated by the mineralogy (Seward, 1972).

Plotting the gold solubilities of the sulfide and chloride complexes on an fO_2 -pH diagram (Figure 26) indicates which of the complexes was capable of transporting the gold. This is determined by noting the solubilities for each complex in the region of the ore solution.

A. Plotting the solubility of the sulfide complex

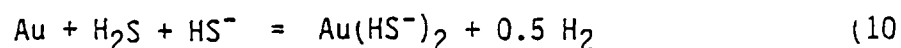
Seward (1972) identified three thio gold complexes contributing to gold solubility. The complex $Au_2(HS)_2S^{-2}$ predominated in alkaline solutions, $Au(HS^-)_2$ in the neutral pH region, and $Au(HS)$ in the acid regions, although its presence was less certain than the first two complexes.

The pH of the ore solution at Erickson was calculated as lying between 3.77 and 5.22. The determination of acidity or alkalinity is complicated by the fact that the dissociation constant of water changes as temperature rises. At higher temperatures, the dissociation of water becomes critically dependent on the density, hence on the pressure, to a greater extent than on temperature. Figure 29 illustrates these changes in the dissociation constant for water for elevated temperatures and for

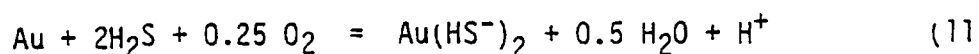
and chromium contents averaged about 2000 ppm and cobalt about 100 ppm. These amounts are very similar to the world average for ultramafic rocks, which characteristically contain 2000 ppm chromium and nickel, and 200 ppm cobalt (Krauskopf, 1979, pp.476-477).

In summary, the crustal setting, mineralogy and trace element geochemistry of the listwanites at Erickson indicates an Alpine-type peridotite parent rock composition. As shown by Figure 28, the mineral assemblages observed at Erickson indicate that the peridotite was serpentinized.

various densities. A dissociation constant of approximately 11.25 corresponds to a temperature of 350 degrees C as indicated in the figure. Therefore, neutral pH at 350 degrees C is approximately 5.6 and perhaps lower since pressures exceeded 600 bars. The ore solution at Erickson is within 1.0 pH unit of neutral, and under these conditions, gold would be transported by the thio complex $Au(HS^-)_2$ according to the reaction:



As H_2S is the dominant sulfur species in the region of the ore solution (see Figure 26), gold transport as this bisulfide complex will occur as:



Log K for this reaction, extrapolated from Barnes (1969) and Casadevall and Ohmoto (1977), is -0.74.

Solving for log K:

$$\log K = \log [Au(HS^-)_2] - pH - 2 \log [H_2S] - 0.25 \log [O_2] \quad (11a)$$

Substituting in values and solving for $\log [O_2]$:

$$\log [O_2] = 10.96 + 4 \log [Au(HS^-)_2] - 4pH \quad (11b)$$

If a value for $[Au(HS^-)_2]$ and pH are arbitrarily assumed, the equation can be solved for $\log [O_2]$. This enables a point to be plotted in fO_2 -pH space. Assuming the same $[Au(HS^-)_2]$ but a different pH, another point can be plotted and the two points joined by a line. This line represents a region in fO_2 -pH space where the solubility is the value assumed for $[Au(HS^-)_2]$. A series of these lines can be constructed for various assumed $Au(HS^-)_2$ concentrations. The slope of the lines will vary according to the dominant sulfur species present in that region. As indicated in the fO_2 -pH diagram (Figure 26), a line corresponding to an $Au(HS^-)_2$ concentration of 10^{-6} moles per liter intersects the region of the ore solution. This complex can therefore transport 10^{-6} moles per

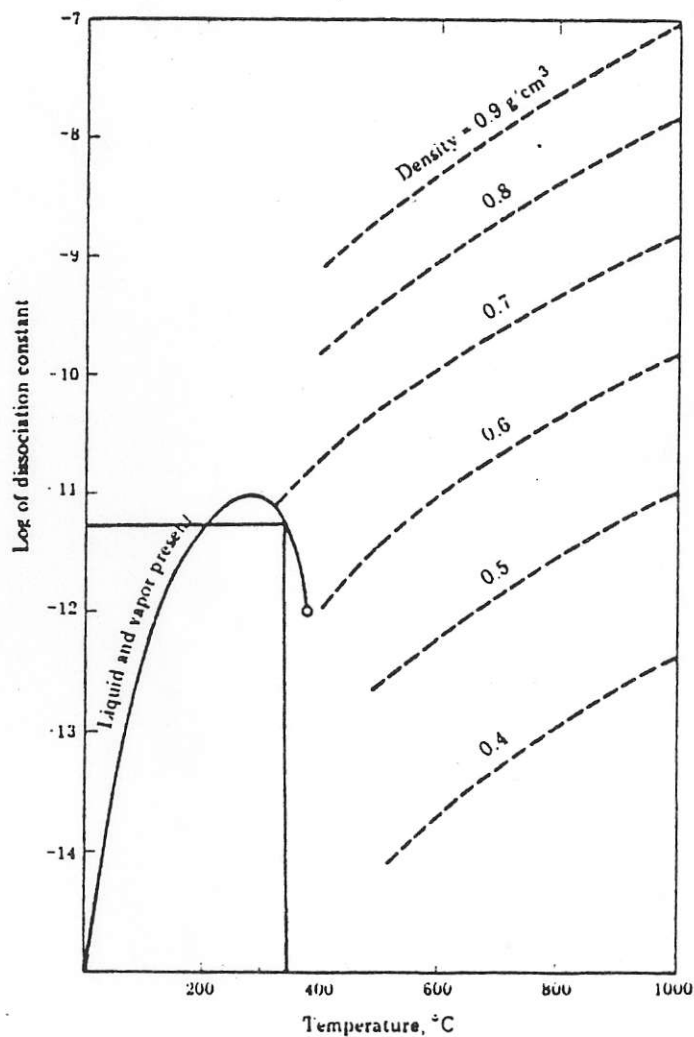


Fig. 29. Ionic dissociation constant of water in high temperature fluids of various densities. The solid curved line is the curve for liquid water under its own vapor pressure. At 350 degrees C the log of the dissociation constant is approximately 11.25. The dashed lines show values of the constant for single-phase fluid water under sufficient pressure to maintain the indicated densities. (After Krauskopf, 1979)

liter or .287 ppm gold.

B. Plotting the solubility of the chloride complex

In saline solutions, gold is transported as a chloride complex according to the reaction:



Log K for this reaction is + 3.95 (Casadevall and Ohmoto, 1977).

Solving for log K:

$$\log K = \log [\text{AuCl}_2] - 0.25 \log [\text{O}_2] + \text{pH} - \log [\text{Cl}^-] \quad (12a)$$

Because NaCl dissociates into its ions by the reaction:



for every mole of Na^+ produced, one mole of Cl^- is produced. The activity of sodium was determined by equation 5 to be 0.213, therefore:

$$[\text{Na}^+] = [\text{Cl}^-] = 0.213 \quad (12c)$$

Substituting this value and +3.95 for log K back into equation 12a and solving for log $[\text{O}_2]$:

$$\log [\text{O}_2] = 4 \log [\text{AuCl}_2] + 4 \text{pH} - 10.44 \quad (12d)$$

As with the bisulfide complex, values for $[\text{AuCl}_2]$ and pH are assumed and the equation solved for log $[\text{O}_2]$. As indicated in Figure 26, the solubility of gold as a bisulfide complex is three orders of magnitude greater than its solubility as a chloride complex.

C. Conclusion

It is apparent from calculation of the solubilities of these complexes, that the bisulfide complex, $\text{Au}(\text{HS}^-)_2$, was the probable transporting agent. Other theoretical gold complexes (e.g. arsenothio) may have transported some gold, but lack of data precludes their evaluation.

IV. Determining the Chemistry of a Fluid In Equilibrium With Serpentinized Peridotite

The chemistry of the ore solution has been roughly calculated and the gold transport complex determined. As the ore solution infiltrates and reacts with the serpentinized peridotite, i.e. during listwanite metasomatism, the chemistry of the ore solution will change affecting gold solubility. In order to determine the chemical changes which take place during fluid mixing and calculate the resultant affect on gold solubility, the chemistry of a fluid in equilibrium with the listwanite parent rock must be determined.

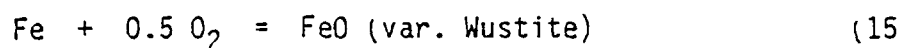
Because serpentinized peridotites commonly contain native metals and sulfur-poor sulfides (Moody, 1976), the oxygen and sulfur fugacities which allow for this condition can be calculated from thermodynamic data available in the literature. In addition, the pH of the fluid can be constrained by constructing a pH-log CO₂ diagram, Figure 28, as well as by reference to chemical analyses of serpentinizing fluids published in the literature.

A. Determination of f_{O_2}

There are three terrestrial environments which are reducing enough for native iron to form: coal deposits, basalt flows which have incorporated coal deposits, and serpentinized peridotites (Frost, 1985). Reduction in the fluid phase associated with serpentinization is caused by the production of magnetite by the reaction:



Native Iron oxidizes to iron oxide according to the reaction:



Log K for reaction 15 interpolated from Robie and Waldbaum (1968) is +18.84. Solving equation 15 for log O_2 :

$$\log [\text{O}_2] = -2 \log K = -37.68 \quad (15a)$$

Another reaction for which there is data is:



Log K for reaction 16 as calculated from the enthalpy and entropy for this reaction listed in Robie and Waldbaum (1968) is +37.2.

Solving equation 16 for log $[\text{O}_2]$:

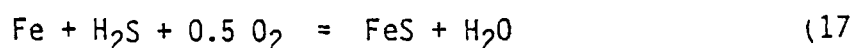
$$\log [\text{O}_2] = -\log K = -37.2 \quad (16a)$$

This is in close agreement with -37.68 as calculated from equation 15a.

The native iron-magnetite (IM) buffer, which is approximately $10^{-37.2}$ moles per liter, is therefore the maximum oxygen fugacity will allow for the existence of native iron.

B. Determination of total sulfur

Sulfur-poor sulfides commonly occur in serpentinized ultrabasic rocks (Moody, 1976). The reaction by which iron sulfide dissociates to sulfur and native iron can be used to determine the sulfur activity of the serpentinizing fluid. Native iron combines with sulfur to form iron sulfide by the reaction:



Log K for this reaction is +26.88 (Robie and Waldbaum, 1968). Solving this equation for log H_2S :

$$\log \text{H}_2\text{S} = -\log K - 0.5 \log [\text{O}_2] \quad (17a)$$

Inserting the values for log K and log $[\text{O}_2]$:

$$\log [\text{H}_2\text{S}] = -8.28 \quad (17b)$$

Native iron, therefore, will form by dissociation of iron sulfide in

a fluid in which total sulfur is very low, equalling or exceeding $10^{-8.28}$.

C. Determination of pH

Figure 28 indicates the range of pH over which serpentine is stable at 25 degrees C and 350 degrees C. It is apparent from this diagram that serpentine is stable under highly alkaline conditions for all temperatures, and alters to talc or talc + magnesite with decreasing pH.

As illustrated by the diagram, at a temperature of 350 degrees C, serpentine can be stable under conditions of pH as low as 4.8. However, experimental work and analyses of serpentinizing fluids indicate that as fluids serpentinize ultramafic rocks, they become extremely alkaline (Moody, 1976). Table II, shows the pH of experimentally derived and naturally occurring serpentinizing fluids. The pH ranges from 8.8 to 12.07, many of which were determined at temperatures in excess of 300 degrees C.

A reasonable estimate of pH for a serpentinizing fluid appears to be fairly alkaline, even at higher temperatures. On this basis, a pH of 9.0 is assumed for the purpose of calculation.

Table II. Experimentally derived serpentinizing fluids compared with the naturally occurring equivalents (After Moody, 1976)

Sample	T, °C	P, bars	Run duration hours	Reacting fluid	Products*	pH**	Mg, ppm	Si, ppm
Run 3-30	311	1470	764	H ₂ O	O (L, C, B, M)	11.6	n.d.	5.0 (4.1)*
Run 3-32	307	1470	911	H ₂ O	L, B, M (O)	10.9	0.39 (.02)	6.1 (2.5)
Run 3-23	323	540	1606	H ₂ O	O (L, C, M)	10.9	0.58 (.03)	4.8 (2.8)
Run 3-22	304	540	1606	H ₂ O	L, C, B, M	11.1	16.20 (.7)	62.4 (21.)
Cazadero A	18	1			O, S	11.77	0.3	0.14
Complexion Spring	10	1			L, C	12.07	0.8	11.2
TC-2**	10	1			A	10.08	0.2	357.0
Aqua de Ney**	10	1			A	10.9	0.3	1870.0
New Idria B	16	1			L, C	8.88	223.0	7.9

Starting materials for the experimental runs were synthetic olivines of varying composition ($Fe_{x_0}-Fe_{y_0}$); details of the experimental work and analytical methods are given in Moody (1974, 1976).

n.d.—not detected, O—olivine, S—serpentine, L—lizardite, C—chrysotile, A—antigorite, B—brucite, M—magnetite.

* For the experiments the phases in parentheses are present in minor amounts; for the natural waters the mineralogy of the rock where the spring is located.

** For the experimental fluids, the measurement of the undiluted fluid at room temperature and pressure immediately after quench, accurate to ± 0.1 pH units.

* One standard deviation.

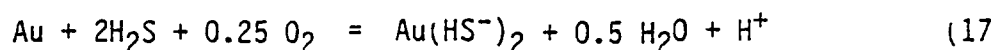
** Spring located at the fault contact between serpentinite and altered dacite, high Si probably due to presence of dacite in contact with an alkaline fluid.

V. Determining the Gold Precipitation Mechanism

The chemistry of both the ore solution and a fluid in equilibrium with the listwanite parent rock have been roughly calculated. Also, the complex which transported gold has been determined. It is presumed that gold solubility dropped during fluid mixing causing its precipitation. In order to calculate the mechanism which caused the gold to precipitate out of solution, the chemical components which affect solubility have to be determined and their relative effect evaluated.

A. Determination of the Chemical Components Affecting Gold Solubility

It was determined that at Erickson gold was transported by the bisulfide complex, $\text{Au}(\text{HS}^-)_2$, according to the reaction:



Rewriting this equation to solve for gold solubility:

$$\log [\text{Au}(\text{HS}^-)_2] = \log K + \text{pH} + 2 \log [\text{H}_2\text{S}] + 0.25 \log [\text{O}_2] \quad (17a)$$

From equation 17a, it can be seen that gold solubility, as the bisulfide complex, is a function of $\log K$, pH, total sulfur and oxygen fugacity. Since $\log K$ is a function of temperature, and chemical reactions are assumed to take place under isothermal conditions, this factor need not be evaluated. The data for both the ore solution and the serpentized peridotite is summarized in Table III.

B. Determining the Gold Precipitation Mechanism

Figure 30 illustrates the sequence of mineralogical zones commonly observed in listwanites between the quartz lodes and the unmetasomatized parent rock, partially serpentized peridotite. As shown in Figure 28, this mineralogical zoning would be produced, at 350 degrees C, by reaction with a CO_2 -rich fluid.

Table III. Summary of fluid composition calculations

	ORE SOLUTION	SERP. PERIDOTITE SOLUTION
pH	4.5	9.0
log ΣS	-1.0	-8.37
log fO_2	-31.0	-37.5

The data from Table III, is illustrated in Figure 30. The activity gradients for the three chemical components, total sulfur, pH and oxygen fugacity are drawn as straight lines between the serpentinized peridotite and quartz lode. Since their exact configuration cannot be evaluated from the data, the lines are only intended to indicate the difference in magnitude of these chemical components in the two fluids.

The relative effect of each chemical component on gold solubility can be evaluated by reference to equation 17a:

$$\log [\text{Au}(\text{HS}^-)_2] = \log K + \text{pH} + 2 \log [\text{H}_2\text{S}] + 0.25 \log [\text{O}_2] \quad (17a)$$

1. Effect of pH on gold solubility

It is apparent from equation 17a, that gold solubility increases proportionately as pH increases. The pH of the ore solution was calculated to lie within the range of 3.77 and 5.22. A median value of 4.5 for the pH of the ore solution is assumed for calculation. The pH of the serpentinized peridotite was estimated to be 9.0. Therefore, during listwanite metasomatism, the pH of the ore solution would increase as the ore solution of pH = 4.5 mixes with the serpentinized peridotite of pH=9.0. It is apparent from equation 17a that this would increase gold solubility. Substituting the values of 4.5 and 9.0 for pH in equation 17a, the increase in solubility as a result of a change in pH from 4.5 to 9.0 is approximately 10^5 moles per liter.

2. Effect of oxygen fugacity on gold solubility

It can be seen from equation 17a that gold solubility increases as oxygen fugacity increases. However, it is intuitively evident, that since $\log[\text{O}_2]$ is multiplied by 0.25, large increases in oxygen fugacity would be required to significantly affect solubility. As table III shows, the

Idealized Listwanite X-Section

qtz Iode	qtz + mag	talc + mag	serp + mag	part. serp. peridotite
-------------	-----------------	------------------	------------------	---------------------------

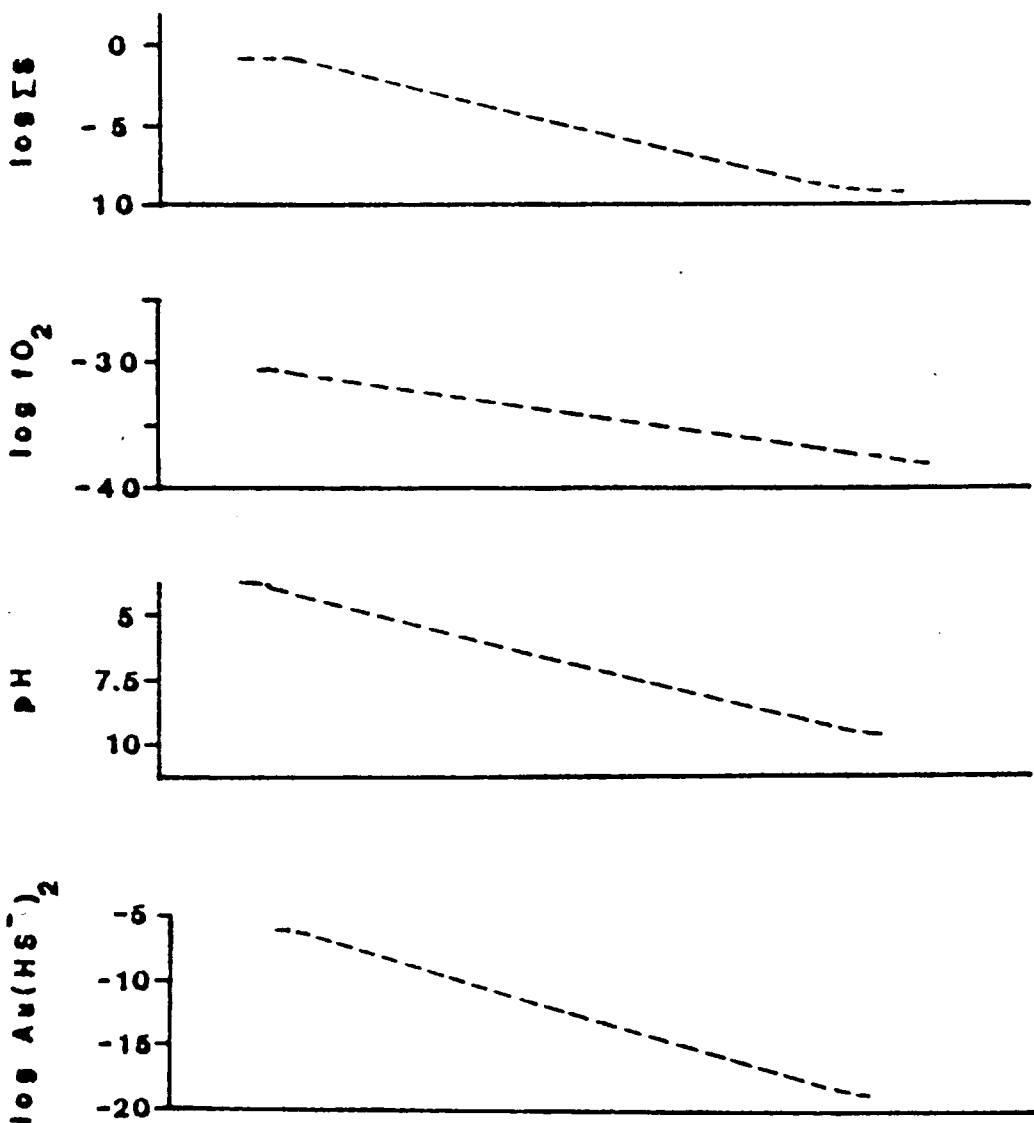


Fig.30 . Model showing activity gradients and resultant gold solubility across a listwanite body.

oxygen fugacity of the ore solution is 10^{-31} moles per liter and the serpentinized peridotite, $10^{-37.5}$ moles per liter. Therefore as the fluids mix, the oxygen fugacity of the ore solution will decrease, thereby decreasing gold solubility and contributing to its precipitation. Substituting the two values for oxygen fugacity back into equation 17a, the decrease in gold solubility as a result of a drop of the fO_2 of the ore solution from 10^{-31} to $10^{-37.5}$ is $10^{0.81}$ moles per liter.

3. Effect of total sulfur on gold solubility

The relatively significant affect of total sulfur on gold solubility is apparent from equation 17a since $\log [H_2S]$ is multiplied by a factor of 2.0 as compared to 1.0 for pH and 0.25 for oxygen fugacity. The total sulfur of the ore solution was calculated to be 10^{-1} and that of the serpentinized peridotite, $10^{-8.37}$. Substituting these values of total sulfur back into equation 17a, a drop in total sulfur by $10^{-7.37}$ will decrease gold solubility $10^{14.74}$ moles per liter.

4. Comparing the relative effect of pH, oxygen fugacity and total sulfur on gold solubility:

The relative effect of the chemical components on gold solubility can be illustrated by a three dimensional, $\log Au (HS^-)_2 - \log \sum S - \log fO_2$ diagram (Figure 31). As discussed, pH would increase during fluid mixing which increases solubility. Therefore, pH is obviously not the mechanism triggering precipitation of gold. Oxygen fugacity would decrease but its effect is relatively small. However, a drop in total sulfur of the ore solution would decrease gold solubility by over 15 orders of magnitude, and this drop in total sulfur is evidently the predominant factor in triggering gold precipitation.

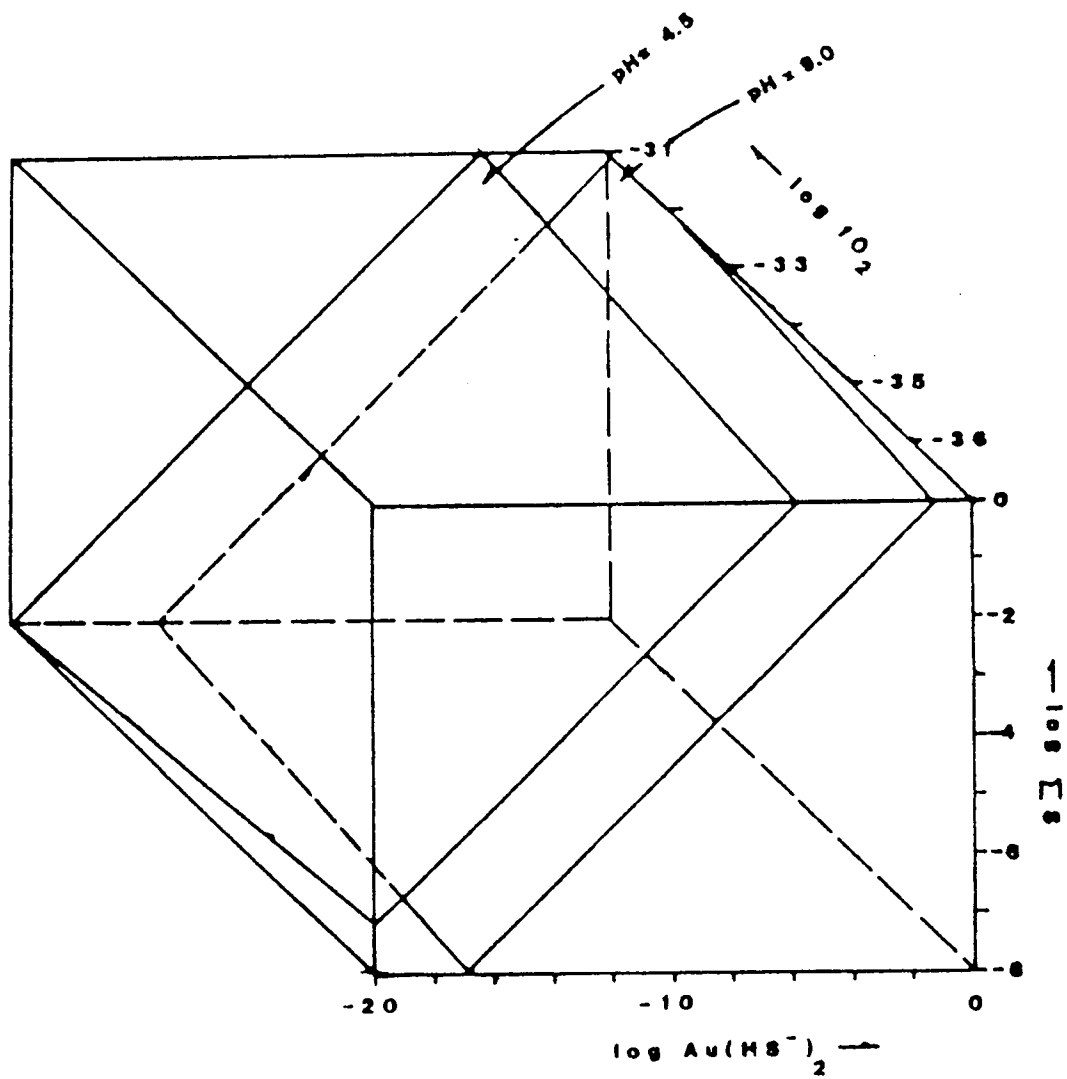


Fig. 31. Three dimensional diagram showing the relative effect of pH, oxygen fugacity and ΣS on gold solubility as $Au(HS^-)_2$.

CONCLUSION

1. The Erickson quartz lodes crystallized from moderately saline solutions under mesothermal conditions. A temperature of 350 degrees C and pressure of 625 atms assumed for the purpose of constructing a model of the system.
2. Gold was transported as the bisulfide complex, $\text{Au}(\text{HS}^-)_2$.
3. The ore solution infiltrated and metasomatized bodies of serpentized peridotite producing a mineralogically zoned, metasomatic rock termed "listwanite".
4. During metasomatism, CaO and Fe_2O_3 were added, SiO_2 and MgO subtracted, from the listwanite parent rock; Al_2O_3 and the minor elements remained relatively immobile.
5. As the ore solution infiltrated and reacted with the listwanite parent rock, the sulfur activity of the ore solution dropped, triggering the precipitation of gold.

REFERENCES CITED

- Azimov, P.T., 1976, Listwanites from the Ziyaetdin Mountains (Western Uzbekistan), Uzb Geol. Zh. No.2 p.41-45: In Chem. Abstr. 85(10)65984y.
- Babcock, R.L., 1973, Computational models of metasomatic processes: Lithos v.6, p. 279-290.
- Barnes, H.L., 1979, ed., Geochemistry of Hydrothermal Ore Deposits: New York, John Wiley and Sons, 774 p.
- Beck, M.E., 1980, Paleomagnetic record of plate-margin tectonic processes along the western edge of North America: Journal of Geophysical Research, v. 85 No. B12, p. 7115-7131.
- Best, M.G., 1982, Igneous and Metamorphic Petrology: San Francisco, W.H. Freeman and Company, 611 p.
- Burt, D.M., and Rose, A.W., 1979, Hydrothermal alteration: In Barnes, H.L., ed., Geochemistry of Hydrothermal Ore Deposits: New York, John Wiley and Sons, p.173-227.
- Casadevall, T., and Ohmoto, H., 1977, Sunnyside Mine, Eureka Mining District, San Juan County, Colorado: Geochemistry of gold and base metal ore deposition in a volcanic environment: Econ. Geol., v. 79, p. 1285-1320.
- Chidester, H., and Cady, W.M., 1972, Origin and emplacement of Alpine-type ultramafic rocks: Nature Physical Science, v.240, p.27-31.
- Collins, P.L., 1979, Gas hydrates in CO₂-bearing fluid inclusions and their use of freezing data for estimation of salinity: Econ. Geol., v. 74, p. 1435-1444.

- Coney, P.J., Jones, D.L., and Monger, J.W.H., 1980, Cordilleran suspect terranes: *Nature*, v. 288, p. 329-333.
- Crerar, D.A., and Barnes, H.L., 1976, Ore solution chemistry v. solubilities of chalcopyrite and chalcocite assemblages in hydrothermal solution at 200 to 350 C: *Econ. Geol.*, v. 71, P. 772-794.
- Diakow, L.J., and Panteleyev, A., 1981, Cassiar Gold Deposits, McDame Map-area (104P/4,5), A summary of field activity: Paper 1981-1, Ministry of Energy, Mines and Petroleum Resources, British Columbia, Canada, p. 55-62.
- Evans, A.M., 1980, *An Introduction to Ore Geology*: New York, Elsevier, 215 p.
- Frost, B.R., 1985, On the stability of sulfides, oxides, and native metals in serpentinite: *Journal of Petrology*, v. 26, Part I, p. 31-63.
- Gabrielse, H., 1963, McDame Map-Area, Cassiar District, British Columbia: *Geological Survey of Canada Memoir 319*, 130 p.
- Gary, M., McAfee, R. Jr., and Wolf, C.L., *Dictionary of Geological Terms*, Revised Edition: Garden City, New York, Anchor Press/Doubleday, 472 p.
- Gordey, S.P., Gabrielse, H., and Orchard, M.J., 1982, Stratigraphy and structure of the Sylvester Allocthon, Southwest McDame Map Area, Northern British Columbia: *Current Research, Part B., Geol. Surv. Can.*, Paper 82-1B, p. 101-106
- Gresens, R.L., 1966, Composition-volume relationships of metasomatism: *Chem. Geol.*, v. 2, p. 47-65.
- Hegelson, H.C., 1969, Thermodynamics of hydrothermal systems at elevated temperatures and pressures: *Amer. Jour. Sci.*, v. 267, No. 7, p. 729-804.

- Hobbs, S.W., and Pecora, W.T., 1941, Nickel-gold deposit near Mount Vernon, Skagit County, Washington: U.S.G.S. Bull 931-D, p. 57-77.
- Hollister, L.S., 1981, Information intrinsically available from fluid inclusions: In Hollister, L.S., and Crawford, M.L., eds., Short Course in Fluid Inclusions: Applications to Petrology: Min. Assoc. Canada, p. 1-9.
- Hollister, L.S., Crawford, M.L., Roedder, R.C., Spooner, E.T.C., and Touret, J., 1981, Practical aspects of microthermometry: In Hollister, L.S. and Crawford, M.L., eds., Short Course in Fluid Inclusions: Applications to Petrology: Min. Assoc. Canada, p. 278-297.
- Holloway, J.R., 1981, Compositions and volumes of supercritical fluids in the earth's crust: In Hollister, L.S. and Crawford, M.L., eds., Short Course in Fluid Inclusions: Applications to Petrology: Min. Assoc. Canada, p. 13-38.
- Kashkai, M.A., and Allakhverdiev, Sh.I., 1971, New data on listwanite and rodingite metasomatites amidst ultrabasites: Izvestiya Akademii Nauk SSSR: Nauka, (Russ), p. 17-26.
- Korzhinskii, D.S., 1970, Theory of Metasomatic Zoning: Clarendon Press, Oxford, 162 p.
- Krauskopf, K.B., 1979, Introduction to Geochemistry: New York, McGraw-Hill, Second Edition, 596 p.
- Monger, J.W.H., Souther, J.G., and Gabrielse, H., 1972, Evolution of the Canadian Cordillera; a plate-tectonic model: Amer. Jour. Sci., v. 272, p. 577-602.
- Moody, J.B., 1976, Serpentinization: a review: Lithos, v. 9, p. 125-138.
- Park, C.F., and MacDiarmid, R.A., 1975, Ore Deposits: San Francisco, W.H.

- Freeman and Company, Third Edition., 511 p.
- Panteleyev, A., 1979, Cassiar Map-Area (104/P): A summary of fieldwork, 1978, Paper 1979-1, Ministry of Energy, Mines and Petroleum Resources, British Columbia, Canada, p. 51-60.
- _____, 1980, Cassiar Map-Area (104/P): A summary of fieldwork, 1979, Paper 1980-1, Ministry of Energy, Mines and Petroleum Resources, British Columbia, Canada, p. 80-88.
- Robie, R.A., and Waldbaum, D.R., 1968, Thermodynamic properties of minerals and related substances at 298.15 K (25 C) and one atm (1.013 bars) pressure and at higher temperatures: U.S.G.S. Bull 1259, 256 p.
- Roedder, E., 1976, Fluid inclusions as samples of ore fluids: In Barnes, H.L. ed., Geochemistry of Hydrothermal Ore Deposits: New York, John Wiley and Sons, p. 684-737
- _____, 1984, Fluid Inclusions, Reviews in Mineralogy, v.12, Min. Soc. of America, 584 p.
- Seward, T.M., 1972, Thio complexes of gold and the transport of gold in hydrothermal ore solutions: Geochim. et Cosmochim. Acta, v. 37, No. 3, p. 379-399.
- Shcherban, I.P., 1966, The origin of listwanites: Doklady Akad. Nauk SSSR, v. 172, p. 149-151.
- Shcherban, I.P., and Borovikova, G.A., 1969, Thermodynamic data on the genesis of listwanites and listwanitized rocks: Doklady Akad. Nauk SSSR., v. 191, p. 218-220.
- Somerville, R., and Basnett, R., 1983, Interim Geological and Development Report on the Erickson Gold Camp, and a Report on the Erickson Gold Mine Ore Reserves: Private company report, Erickson Gold Mining Corp., Vancouver, British Columbia, Canada.
- Storms, W.H., 1899, Mariposa County's mineral wealth: In Benjamin, E.H.,

- California Mines and Minerals: California Miners Association, Souvenir Edition, p. 361-369.
- Stul'chikov, V.A., Sharkin, O.P., Samoilovich, I.G., and Bondarenko, I.N., 1982, Sulfide mineralization of listwanites in ultrabasic rocks of the Verkhovtsevo syncline: In Chem. Abstr. 97(2)9307r.
- Turner, F.J., 1981, Metamorphic Petrology: New York, McGraw-Hill Book Company, Second Edition, 524 p.
- Williams, H., Turner, F.J., and Gilbert, C.M., 1982, Petrography: An Introduction to the Study of Rocks in Thin Sections: San Francisco, W.H. Freeman and Company, Second Edition, 598 p.
- Wittkopp, R.W. 1980, A hypothesis for the localization of gold in quartz veins, Alleghany District, California: In Loyd, R.C., and Rapp, J.S., eds., Mineral Resource Potential of California, Sierra Nevada Section, Society of Mining Engineers, AIME, Conference Transactions (March 27-28, 1980), Sacramento, California, p. 9-22.

Appendix I

Geochemical analyses for major and minor elements. Sample 0113 is serpentinized peridotite

<u>SAMPLE NUMBER</u>	<u>SiO₂</u>	<u>Al₂O₃</u>	<u>Fe₂O₃</u>	<u>TiO₂</u>	<u>MgO</u>	<u>CaO</u>	<u>Na₂O</u>	<u>K₂O</u>	<u>P₂O₅</u>	<u>LOI</u>
L-1	40.04	0.91	7.43	0.07	28.79	5.09	0.03	0.03	0.03	15.71
L-2	33.04	10.93	12.15	1.37	29.62	0.84	0.04	0.04	0.12	12.31
L-3	9.76	0.67	5.72	0.04	17.14	25.97	0.02	0.02	0.05	38.90
L-4	28.58	0.79	6.69	0.07	21.28	8.64	0.03	0.03	0.06	31.01
L-5	39.25	0.84	6.09	0.05	28.96	2.53	0.03	0.03	0.03	20.34
L-6	33.03	0.71	5.52	0.04	25.44	6.88	0.03	0.03	0.04	25.87
L-7	42.64	5.12	6.24	0.31	9.08	12.81	0.03	0.05	0.19	22.01
L-8	61.90	1.03	3.90	0.03	6.37	9.82	0.03	0.03	0.05	15.23
L-9	50.22	2.39	8.80	0.08	6.14	10.22	0.03	0.17	0.07	17.48
L-10	46.19	1.26	7.73	0.03	7.84	12.65	0.03	0.03	0.08	21.32
L-11	40.11	0.84	6.96	0.09	13.10	11.50	0.03	0.03	0.07	25.91
L-12	20.12	0.25	11.56	0.04	20.27	10.57	0.03	0.03	0.05	34.59
L-13	8.84	0.11	12.59	0.02	14.40	22.18	0.02	0.02	0.09	37.59
L-14	46.02	0.05	5.15	0.05	13.57	9.84	0.03	0.03	0.06	23.83
L-15	51.89	0.25	4.14	0.05	8.60	12.81	0.03	0.03	0.06	20.45
L-16	34.59	5.63	3.81	0.04	10.27	16.42	0.03	0.03	0.09	27.28
0113	40.23	0.50	3.69	0.02	41.46	0.03	0.02	0.02	0.03	13.41

Appendix I Continued

Geochemical analyses for trace elements

SAMPLE NUMBER	Ni ppm	Co ppm	Cr ppm	Au ppb	Hf ppm	Th ppm	Zr ppm
L-1	2050	112	1900	1	1	1	89
L-2	----	---	----	-	-	-	--
L-3	----	---	----	-	-	-	--
L-4	----	---	----	-	-	-	--
L-5	2100	96	1750	4	1	1	35
L-6	----	---	----	-	-	-	--
L-7	----	---	----	-	-	-	--
L-8	1900	112	2100	14	1	1	34
L-9	----	---	----	-	-	-	--
L-10	----	---	----	--	-	-	--
L-11	----	---	----	--	-	-	--
L-12	----	---	----	--	-	-	--
L-13	----	---	----	--	-	-	--
L-14	----	---	----	--	-	-	--
L-15	----	---	----	--	-	-	--
L-16	----	---	----	--	-	-	--
0113	2380	59	2000	1	1	1	32

Appendix II

Fluid-inclusion data for Maura and Alison veins

Vein	Inclusion #	H ₂ O solid- liquid	H ₂ O vap - liquid
Maura	M-1A-1	-5.9 C	203 C
	M-1A-2	-5.3 C	251 C
	M-2A-1	-7.4 C	252 C
	M-2A-2	----	220 C
	M-2B-2	----	325 C
	M-2B-3	----	312 C
	M-2B-5	----	351 C
	M-2B-6	----	323 C
	M-4A-1	----	230 C
	M-4A-2	----	277 C
	M-4A-3	----	248 C
	M-6A-1	----	312 C
	M-6A-2	----	320 C
	M-6A-3	----	297 C
	M-6A-4	----	326 C
	M-6A-5	----	339 C
	M-6A-6	----	300 C
	M-6A-7	----	339 C
	M-6A-9	----	357 C
	M-7A-1	----	333 C
	M-7A-2	----	310 C
	M-8A-1	----	268 C
	M-8A-2	----	269 C
	M-8A-3	----	243 C
	M-8A-4	----	278 C
	M-8A-5	----	283 C
	M-8A-6	----	257 C
	M-8A-7	----	255 C
	M-8B-1	-5.5 C	239 C
	M-8B-2	-4.2 C	decrep.
	M-8B-3	-6.6 C	decrep.

Appendix II continued

Vein	Inclusion #	H ₂ O solid - liquid	H ₂ O vap - liquid
Alison	A-2A-1	-6.0 C	241.0 C
	A-2A-2	-6.4 C	239.0 C
	A-2B-1	-7.8 C	231.6 C
	A-2B-2	---	218 C
	A-2B-3	---	292 C
	A-2B-4	---	285 C
	A-2B-5	---	287 C
	A-2B-6	---	279 C
	A-2B-7	---	285 C
	A-2B-8	---	287 C
	A-2B-9	---	277 C
	A-2B-10	---	288 C
	A-2B-11	---	296 C
	A-2B-12	---	279 C
	A-2B-13	---	288 C
A-2B-14	---	288 C	

Appendix III

Minerals present in samples L-1 through L-16 as indicated by X-ray diffractometer in conjunction with thin-section analysis.

<u>Sample Nbr.</u>	<u>Major mineral phases</u>	<u>Accessory minerals</u>
L-1	dolomite talc lizardite quartz	calcite ferrospinel tremolite
L-2	diabantite (chl) antigorite talc quartz magnesite	cobaltite ilmenite magnetite
L-3	dolomite antigorite quartz kammererite (chl)	ilmenite
L-4	dolomite magnesite antigorite diabantite	ilmenite diopside lizardite magnetite or chromite
L-5	talc magnesite	dolomite diabantite or kammererite quartz ferrospinel or cobaltite
L-6	dolomite magnesite talc diabantite antigorite	quartz ferrospinel
L-7	quartz dolomite kammererite	Cr-mica* ferrospinel chromite

* No X-ray data available - presence evident in thin-section and in hand specimen.

Appendix III Continued

<u>Sample Nbr.</u>	<u>Major mineral phases</u>	<u>Accessory minerals</u>
L-8	quartz dolomite kammererite	pyrite magnesite Cr-mica
L-9	quartz kammererite dolomite	pyrite Cr-mica
L-10	quartz dolomite pyrite	nimite (chl) Cr-mica antigorite
L-11	quartz dolomite magnesite	pyrite spinel Cr-mica
L-12	quartz dolomite magnesite	pyrite Cr-mica
L-13	quartz dolomite magnesite	pyrite Cr-mica
L-14	quartz dolomite magnesite	chrysotile or antigorite or kammererite pyrite Cr-mica
L-15	quartz dolomite	cobaltite spinel magnesite pyrite
L-16	quartz dolomite	nimite and/or diabantite magnetite Cr-mica